isvr Institute of Sound and Vibration Research

Proportional, Integral, Derivative, PID-, PI- and PD- Velocity Feedback Control with Inertial Actuators

C. Gonzalez Diaz and P. Gardonio

ISVR Technical Memorandum No 956

December 2005

University of Southampton

SCIENTIFIC PUBLICATIONS BY THE ISVR

Technical Reports are published to promote timely dissemination of research results by ISVR personnel. This medium permits more detailed presentation than is usually acceptable for scientific journals. Responsibility for both the content and any opinions expressed rests entirely with the author(s).

Technical Memoranda are produced to enable the early or preliminary release of information by ISVR personnel where such release is deemed to the appropriate. Information contained in these memoranda may be incomplete, or form part of a continuing programme; this should be borne in mind when using or quoting from these documents.

Contract Reports are produced to record the results of scientific work carried out for sponsors, under contract. The ISVR treats these reports as confidential to sponsors and does not make them available for general circulation. Individual sponsors may, however, authorize subsequent release of the material.

COPYRIGHT NOTICE

(c) ISVR University of Southampton All rights reserved.

ISVR authorises you to view and download the Materials at this Web site ("Site") only for your personal, non-commercial use. This authorization is not a transfer of title in the Materials and copies of the Materials and is subject to the following restrictions: 1) you must retain, on all copies of the Materials downloaded, all copyright and other proprietary notices contained in the Materials; 2) you may not modify the Materials in any way or reproduce or publicly display, perform, or distribute or otherwise use them for any public or commercial purpose; and 3) you must not transfer the Materials to any other person unless you give them notice of, and they agree to accept, the obligations arising under these terms and conditions of use. You agree to abide by all additional restrictions displayed on the Site as it may be updated from time to time. This Site, including all Materials, is protected by worldwide copyright laws and treaty provisions. You agree to comply with all copyright laws worldwide in your use of this Site and to prevent any unauthorised copying of the Materials.

UNIVERSITY OF SOUTHAMPTON

INSTITUTE OF SOUND AND VIBRATION RESEARCH

SIGNAL PROCESSING & CONTROL GROUP

Proportional, Integral, Derivative, PID-, PI-, and PD-Velocity Feedback Control with Inertial Actuators

by

C. González Díaz and P. Gardonio

ISVR Technical Memorandum N° 956

December 2005

Authorised for issue by
Prof R Allen
Group Chairman

© Institute of Sound & Vibration Research

ABSTRACT

This report presents a comprehensive study of feedback active control with inertial actuators to reduce the vibrations of mechanical systems. The basic Single Degree of Freedom (SDOF) vibration transmission problem is considered first in order to highlight the physics of the following velocity feedback control functions: a) Proportional feedback for the implementation of velocity control that generates active damping, b) Integral feedback for the implementation of displacement control that generates active stiffness, c) Derivative feedback for the implementation of acceleration control that generates active mass, e) PID feedback for the implementation of velocity – displacement – acceleration control that generates active damping – stiffness – mass, f) PI feedback for the implementation of velocity – displacement control that generates active damping – stiffness and g) PD feedback for the implementation of velocity – acceleration control that generates active damping – mass. The control effects generated by an inertial force actuator and an inertial electro–dynamic actuator are then studied with reference to the six control laws listed above. This analysis is focussed on two problems: first the vibration control of a SDOF mechanical system and second the vibration control of a flat plate distributed system. Both analyses are carried out in three stages: first a mobility model is derived, second a stability analysis is presented with reference to the Nyquist stability criterion and third the control performances are assessed.

TABLE OF CONTENTS

TABLE OF FIGURES

LIST OF TABLES

1. INTRODUCTION.

This report is concerned with the study of inertial actuators for smart panels with a decentralised feedback control system for the implementation of Active Structural Acoustic Control (ASAC). In particular this report summarises a comprehensive study of Single Input Single Output (SISO) active feedback control schemes using inertial actuators.

In many engineering systems it is important to control the transmission of vibration from a source of disturbance to other devices or to the environment since it might result in discomfort and loss of efficiency. In particular vibration of panels and shell structures may generate high levels of noise which could be a problem in many applications, particularly in transportation vehicles such as aircrafts, helicopters, cars, trains, etc. Therefore the background of this study is the control of vibration of thin panels to avoid the excessive radiated noise. Vibration and sound radiation control can be achieved with passive means such as mass damping and stiffness treatments applied on the radiating structure [1]. These methods have been proved to be efficient in the high audio frequency range. However, they have little effect in the low audio frequency range, where the response of the sound radiating structures are characterised by well–separated resonances [1]. In order to control vibration and sound radiation in the low frequency range, active control methods have been considered. Frequently both systems, passive and active, are used in parallel to improve the vibration control and to reduce the sound radiation.

Active control architectures can be divided into two groups: feedforward and feedback control systems. In feedforward control there is a principal problem; a reference signal should be known far enough in advance otherwise this control system is inefficient [2]. In this case feedback control schemes should be utilized. In fact, in feedback control systems the reference signal is not necessary and the sensors and actuators are closely attached or even can be embedded in the structure to be controlled. Feedback control systems can be classified in three categories: a) Multiple Input Multiple Output (MIMO) systems with fully coupled arrays of error sensor and actuators, b) Decentralised MIMO feedback control schemes with arrays of independent sensor–actuator pairs and c) SISO active feedback control schemes, using distributed sensor–actuator pairs.

The fully coupled MIMO feedback systems are difficult to implement in practice, since a reliable model of the response functions between all sensors and actuators is required by the controller [3,4]. Elliott at al. [5] have shown that decentralised MIMO

control gives quite good results which are comparable to those that would be obtained from an ideal fully coupled MIMO feedback control system when the sensor–actuator response functions are available. The implementation of MIMO decentralised systems is much simpler than that of fully coupled systems, since simple SISO feedback loops needs to be implemented. Elliott at al. [5] have shown that, provided the sensor–actuator pairs are dual and collocated [6,7] then the system is bound to be stable if proportional control is implemented. Therefore, the main issue of MIMO decentralised control is concerned with the design of collocated and dual sensor–actuator pairs. Moreover Elliott at al. [5] have shown than, when decentralised velocity feedback loops are implemented in such a way as to synthesize active dampers, then, provided an optimal gain is implemented in such a way the damping action is maximised without priming the structure at the control position, both the frequency average vibration and sound radiation of the structure are reduced. This is because the optimal tuned active dampers reduce the amplitudes of the well separated low frequency resonance of the structure which control the frequency averaged vibration and sound radiation of the structure at the low frequency bands. In principle SISO feedback control systems using distributed sensor–actuator pairs specifically designed to minimise the most efficient radiations modes [8] form the simplest and most convenient solution. However, they normally require strain transducers, such as piezoelectric transducers, which can not be easily used in matched pairs as sensors and actuators since their coupling is affected by the in–plane strain effect that "covers" the coupling via the bending vibration of the structure to be controlled [9]. In conclusion MIMO decentralised systems offers a good compromise between the fully coupled MIMO and the SISO with distributed sensors control systems. The main issue of this strategy is the design of collocated and dual sensor actuator pairs.

In this report the attention is focused on the design of inertial force actuators with velocity sensors at their base. In particular the stability issues and control performance effects of one control unit are studied with reference to the most common feedback control functions:

a) Proportional Control for implementation of Velocity Feedback,
b) Integral Control for implementation of Displacement Feedback
c) Derivative Control for implementation of Acceleration Feedback and
d) PID Control (Proportional–Integral–Derivative Feedback Control).

This report is subdivided in three chapters. Chapter 2 presents the main features of SISO feedback control with reference to the fundamental problem of vibration isolation in a SDOF mechanical system. Chapter 3 introduces the control of a mechanical system using an inertial actuator. For simplicity the system under control is modelled

with a SDOF system. Thus the complete system including the inertial control actuator is modelled with two DOF. Finally in chapter 4, the control of a distributed system, such as a flat plate, is considered. In order to better understand the physics of the system, four models are considered where the feedback control loops refer to an ideal sky–hook reactive force actuator, a practical inertial force actuator and an inertial electro–dynamic actuator with either current or voltage control.

The study presented in the three chapters is organised in a consistent structure which first introduces the mathematical model for the various control schemes, it then presents the stability analysis using the Nyquist criterion for SISO control loops [10] and finally it gives the control performance results for all control schemes.

2. FUNDAMENTAL CONCEPTS OF FEEDBACK CONTROL.

In this chapter, the steady–state response of a SDOF active vibration control system under harmonic excitation of the base will be considered. First, the response of this system will be studied when there is no active vibration control assuming different values of damping ratio. Second, the effect of a feedback control loop will be examined assuming a small damping ratio. A number of control architectures will be studied namely: a) Proportional Control for implementation of Velocity Feedback, b) Integral Control for implementation of Displacement Feedback c) Derivative Control for implementation of Acceleration Feedback and d) PID Control (Proportional–Integral–Derivative Feedback Control).

2.1 SDOF under harmonic motion of the base.

Figure 1(a) shows the notation used for the mass–spring–dashpot SDOF system considered in this chapter. In this report the mechanical cinematic (displacement, velocities, accelerations) or kinetic (force) functions have been taken to be time–harmonic and given by the real part of counterclockwise rotating complex vectors (phasors), so that, for example the displacement and force functions are given by $x(t) = \mathrm{Re}\{X(\omega)e^{j\omega t}\}$, $f(t) = \mathrm{Re}\{F(\omega)e^{j\omega t}\}$, where ω is the circular frequency [rad/s] and $j = \sqrt{-1}$. Therefore $x(t)$ and $f(t)$ are the time–dependent harmonic and force function while $X(\omega)$ and $F(\omega)$ are the complex frequency–dependent displacement and force phasors. In order to simplify the formulation, the harmonic time dependence is assumed in the mathematical expressions. Also, the first and second derivative of the time–harmonic functions will be represented by velocity and acceleration frequency dependent phasors; $\dot{X}(\omega) = j\omega\, X(\omega)$ and $\ddot{X}(\omega) = -\omega^2 X(\omega) = j\omega\, \dot{X}(\omega)$.

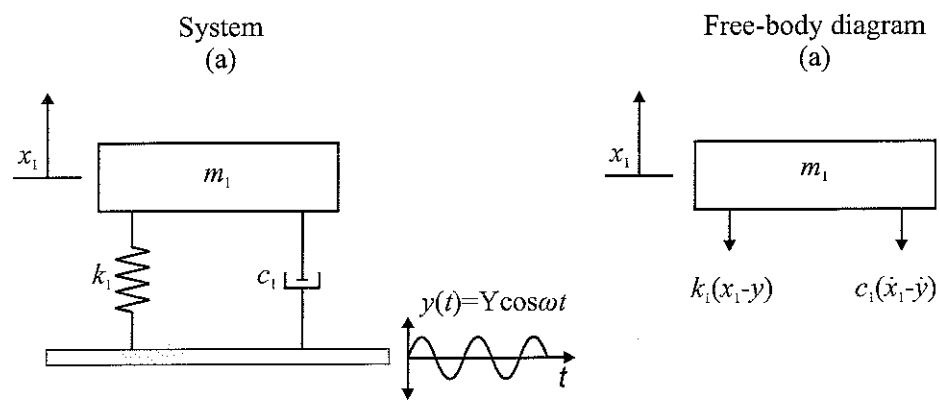

Figure 1: *Single degree of freedom system under harmonic motion of the base.*

Considering the free–body diagram shown in Figure 1(b) above and using Newton's second law of motion ($\sum F = m_1\ddot{x}_1$), the following equation of motion is obtained:

$$m_1\ddot{x}_1 + c_1\dot{x}_1 + k_1x_1 = c_1\dot{y} + k_1y, \tag{2.1}$$

where m_1 is the inertial mass, c_1 is the damping coefficient, k_1 the stiffness, x_1 is the displacement of the inertial mass and the base excitation is given by:

$$y = \mathrm{Re}\left\{ Ye^{j\omega t} \right\}, \tag{2.2}$$

where Y is the amplitude. The right hand side of the Eq. (2.1) base can be seen as a force $f(t)$ acting on a "classic" SDOF mass–spring–dashpot system with a rigid base:

$$f = c_1\dot{y} + k_1y \ . \tag{2.3}$$

The steady state solution of Eq. (2.1) can be found by assuming:

$$x_1(t) = \left\{ X_1e^{j\omega t} \right\} . \tag{2.4}$$

By substituting Eq. (2.4) into Eq. (2.1) and solving for X_1, the following relation between the phasors of the mass and base displacement is obtained:

$$X_1(\omega) = \frac{k_1 + jc_1\omega}{k_1 - m_1\omega^2 + j\omega c_1}Y(\omega) \ . \tag{2.5}$$

Figure 2 shows the variation of the ratio between the velocity of the inertial mass and the displacement of the base calculated assuming the physical parameters given in Table 1 and for different damping ratios; $\xi = c/c_c$ where c_c is the critical damping:

$$c_c = 2m_1\omega_n \ , \tag{2.6}$$

and ω_n is the natural frequency:

$$\omega_n = \sqrt{\frac{k_1}{m_1}} \ . \tag{2.7}$$

Table 1: *Physical parameters for the elements in the SDOF system.*

Parameter	Value
Critical Damping	$c_c = 2.83$ N/ms^{-1}
Mass	$m_1 = 0.015$ Kg
Stiffness	$k_1 = 133.24$ N/m
Natural frequency	$f_n = 10$ Hz

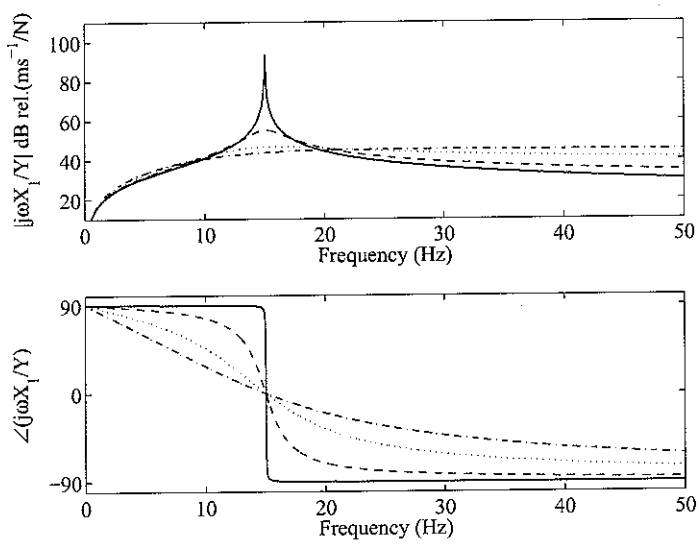

Figure 2: *Modulus and phase of the ratio between the velocity of the inertial mass and the displacement of the base of the system shown in Figure 1(a) when the system is damped by a ξ_1=0.001 (solid line), ξ_2=0.1 (dashed line), ξ_3=0.4 (dotted line) or ξ_4=0.8 (dash-dot line).*

The key features of the SDOF system under study can summarised in the following points:

- For an undamped system (ξ=0) $|j\omega X_1/Y|$ tents towards infinity at resonance.
- The addition of small amounts of damping lead to important reductions of the response at, or near, resonance but also increase the response at frequencies much higher than resonance.
- Increasing damping causes the frequency of maximum response to move to lower values.
- Increasing the amount of damping leads to a smoother phase transition.

Assuming the SDOF represents an isolation system, the results shown in Figure 2 indicate that, in order to obtain the maximum vibration reduction, the spring element should be selected in such a way as to keep the natural frequency as low as possible in respect to the limitation imposed on the static displacement $\delta = m_1 g / k_1$, where g is the acceleration due to the gravity, which also depends on the stiffness of the spring. Also the damping effect should be as small as possible, although also in this case a compromise must be found in order to avoid excessive vibrations transmission around the resonance frequency.

2.2 SDOF under harmonic motion of the base with a Feedback control loop.

The design problems highlighted above generate important limitations to the low frequency passive isolation effect introduced by the spring–dashpot element. An interesting and effective way to enhance the vibration isolation is the implementation of an active control system. In this section the effects produced by a feedback control system, which, as shown in Figure 3(a), is composed by a) a control sensor that measures the velocity of the mass, b) a control actuator mounted in parallel with the spring–dashpot elements that produces reactive forces between the mass and base and c) a control system that implement a control function $-H$ which in the simplest case is given by a pure gain, $-g$.

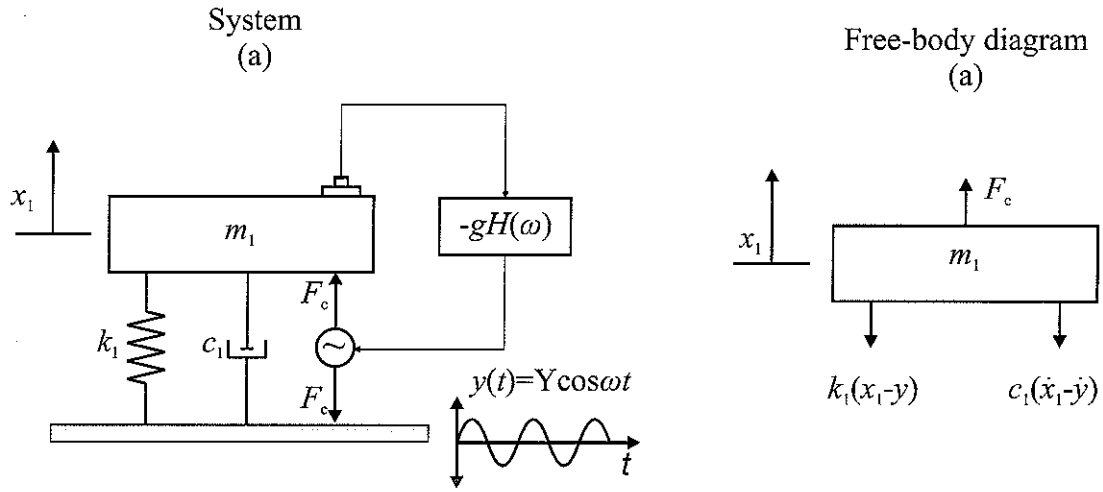

Figure 3: *SDOF under harmonic motion in the base with feedback control.*

The equation of motion for the system shown in Figure 3(a) with a Proportional, Integral, Derivative, or combination among the three, Control functions can be derived

from the free-body diagram shown in Figure 3(b) using Newton's second law of motion, which gives:

$$m_1\ddot{x}_1 + c_1\dot{x}_1 + k_1x_1 = c_1\dot{y} + k_1y + f_c, \tag{2.8}$$

where $f_c = \mathrm{Re}\{F_c e^{j\omega t}\}$ is the feedback reactive control force which depends on the control loop used as described in the points below

- Proportional Control for implementation of velocity Feedback; in this case, the output signal from the velocity sensor is feedback to the actuator via a negative control gain -g, so that the phasor of the control force F_c, is directly proportional to the opposite of the velocity of the mass:

$$F_c = -g\dot{X}_1(\omega)\ . \tag{2.9}$$

  Therefore substituting the steady state solution $x_1(t) = \{X_1 e^{j\omega t}\}$, (Eq. (2.4)) into the equation of motion (Eq.(2.1)), with $y = Ye^{j\omega t}$, and $F_c = -g\dot{X}_1(\omega)$, the following expression for the complex amplitude of the response is obtained:

$$X_{1-P}(\omega) = \frac{k_1 + jc_1\omega}{k_1 - m_1\omega^2 + j\omega(c_1 + g)}Y(\omega). \tag{2.10}$$

  The denominator of this equation indicates that Proportional Control adds active damping. This effect will be further discussed in Section 2.1 where simulations results for this control schema are presented.

- Integral Control for implementation of displacement Feedback; in this case, the output signal from the velocity sensor is feedback to the actuator via a negative integral control function $-g/j\omega$, so that the phasor of the control force F_c is directly proportional to the opposite of the displacement of the mass. Hence F_c is given by:

$$F_c = -g\frac{\dot{X}_1(\omega)}{j\omega} = -gX_1(\omega)\ . \tag{2.11}$$

  Following the same procedure as in the previous point, the complex response is found to be in this case:

$$X_{1-I}(\omega) = \frac{k_1 + jc_1\omega}{(k_1 + g) - m_1\omega^2 + j\omega c_1}Y(\omega). \tag{2.12}$$

The denominator indicates that Integral Control adds active stiffness so that the resonance frequency is moved to higher values as it will be further discussed in section 2.4.

- Derivative Control for implementation of acceleration Feedback: in this case, the output signal from the velocity sensor is feedback to the actuator via a derivative control function $-j\omega g$, so that the phasor of the control force F_c, is directly proportional to the opposite of the acceleration of the mass. Hence F_c is given by:

$$F_c = -j\omega g\dot{X}_1(\omega) = -g\ddot{X}_1(\omega) \ . \tag{2.13}$$

Once more, following the procedure highlighted in the previous points the response is found to be:

$$X_{1\text{-}D}(\omega) = \frac{k_1 + jc_1\omega}{k_1 - (m_1 + g)\omega^2 + j\omega c_1} Y(\omega) \ . \tag{2.14}$$

The denominator shows in this case that Derivative Control adds active mass which moves the resonance frequency to lower values as it will be shown in section 2.4.

As it will be shown in the following section 2.4: a) Velocity Feedback Control (Proportional Control) can control the response at resonance, b) Displacement Feedback Control (Integral Control) can reduce vibration at low frequency below resonance and c) Acceleration Feedback Control (Derivative Control) can reduce vibration at higher frequency above resonance. Thus a combination of these three control approaches; Proportional–Integral–Derivative Feedback Control (PID), is expected to enhance the vibration isolation in all frequency range of interest.

- Proportional–Integral–Derivative (PID) Control; in this case, the output signal from the velocity sensor is feedback to the actuator via a control function combining proportional, integral and derivative control so that, the phasor of the control force F_c is directly proportional to the opposite of the velocity–displacement–acceleration of the mass. Hence F_c is given by:

$$F_c = \left\{-k_P - \frac{k_I}{j\omega} - j\omega k_D\right\}\dot{X}_1(\omega) = -k_P\dot{X}_1(\omega) - k_I X_1(\omega) - k_D\ddot{X}_1(\omega) \ , \tag{2.15}$$

where k_P, k_I and k_D are the proportional, the integral and the derivative constants respectively. Following the procedure seen above the response is found to be:

$$X_{1\text{-}PID}(\omega)=\frac{k_1+jc_1\omega}{(k_1+g_I)-(m_1+g_D)\omega^2+j\omega(c_1+g_P)}Y(\omega)\ . \qquad (2.16)$$

The numerator shows that PID Control adds active damping, active stiffness and active mass so that vibration reduction can be obtained in the three regions, below, at and above resonance as it will be shown in the section 2.4.

2.3 Stability analysis.

A critical problem for the design of feedback control system is stability. To address the problem of stability, several graphical techniques have been developed for Single Input Single Output control schemes. Two of these techniques are the *Bode* and *Nyquist plots* [11]. The first one consists of plotting the magnitude versus frequency and phase angle versus frequency of the open loop sensor–actuator frequency response function. The second one is a polar plot of the open loop sensor–actuator frequency response function as ω varies from $-\infty$ to ∞. Both of them rely on the Nyquist stability criterion which state that "*provided the Nyquist plot of the open loop sensor–actuator frequency response does not encircle the Nyquist point –1+j0, then the control system is stable*". Therefore in those cases where the sensor–actuator frequency response function enters on the left hand side quadrants of the Nyquist plot, a limited range of control gains can be implemented, so that the system is said to be conditionally stable. If instead the Nyquist plot of the sensor–actuator response function occupies only the right hand side quadrants of the Nyquist plot, i.e. the response function is strictly positive real, then the system is unconditionally stable. The same type of conclusion can be drawn by considering the Bode plot of the open loop sensor–actuator response function. If the phase plot is confined between ±90° then the open loop sensor–actuator response function is real positive and thus the system is unconditionally stable. If the phase plot exceed ±90° then the system could be either conditionally stable or indeed unstable. Normally the concepts of gain and phase margin [1] are used to assess the level of stability.

There are two necessary requirements in order to have an unconditionally stable system: the sensor–actuator pair must be dual and collocated [6,7]. Indeed in this case the sensor–actuator frequency response function is real positive definite so that its Nyquist plot occupies the right hand side quadrants as ω varies from $-\infty$ to $+\infty$ and thus the Nyquist instability point is never encircled whatever the control gain.

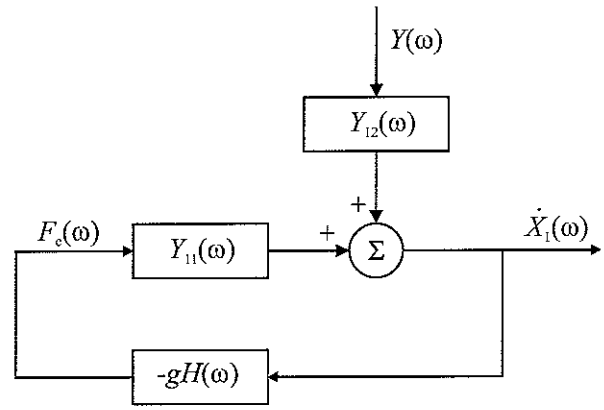

Figure 4: *Block diagram of feedback control system implemented on the SDOF system.*

The response of the active system shown in Figure 3 can be formulated in terms of mobility frequency response functions: *Y=velocity/force.* In this case, as shown by the block diagram in Figure 4, the response at the error sensor can be modelled in terms of the primary disturbance effect plus the closed feedback loop effect. This is a classical disturbance rejection control loop. Considering Figure 4 the following expressions for $\dot{X}_1$ and control force F_c are obtained:

$$\dot{X}_1 = Y_{12}Y + Y_{11}F_c \ , \tag{2.17}$$

$$F_c = -gH(\omega)\dot{X}_1 \ , \tag{2.18}$$

where, the mobility functions Y_{12} and Y_{11} are given by:

$$Y_{12} = \left.\frac{\dot{X}_1}{Y}\right|_{F_c=0} = j\omega \frac{k_1 + jc_1\omega}{k_1 - m_1\omega^2 + j\omega\, c_1} \ , \tag{2.19}$$

$$Y_{11} = \left.\frac{\dot{X}_1}{F_c}\right|_{Y=0} = j\omega \frac{1}{k_1 - m_1\omega^2 + j\omega\, c_1} \ , \tag{2.20}$$

and $H(\omega)$ is a control function. Substituting Eq. (2.18) into Eq.(2.17), and solving respect the velocity $\dot{X}_1$, the following expression is obtained:

$$\dot{X}_1 = \frac{Y_{12}}{1 + gHY_{11}} Y \ , \tag{2.21}$$

where HY_{11} is the open loop frequency response function between the velocity sensor and the control actuator. If Re(HY_{11})>0, then Eq. (2.21) shows that $\dot{X}_1 / Y < 1$ for any control gain and frequency, that is the feedback control monotonically reduces the velocity of the system. Unconditionally stable control systems allow large control gains without causing instability and hence may achieve superior control performance.

In the following sub–sections the stability for the different control architectures listed above is studied.

§ Proportional Control. Velocity Feedback.

In order to implement negative velocity feedback, the output signal from the velocity sensor is feedback to the actuator via a negative proportional control function; $H(\omega)$= $-g$, and thus:

$$F_c = -g\dot{X}_1 \ , \tag{2.22}$$

Figure 5 shows the amplitude–phase and Nyquist plot of the open loop sensor–actuator frequency response function HY_{11} in the frequency range between 0 and 50 Hz.

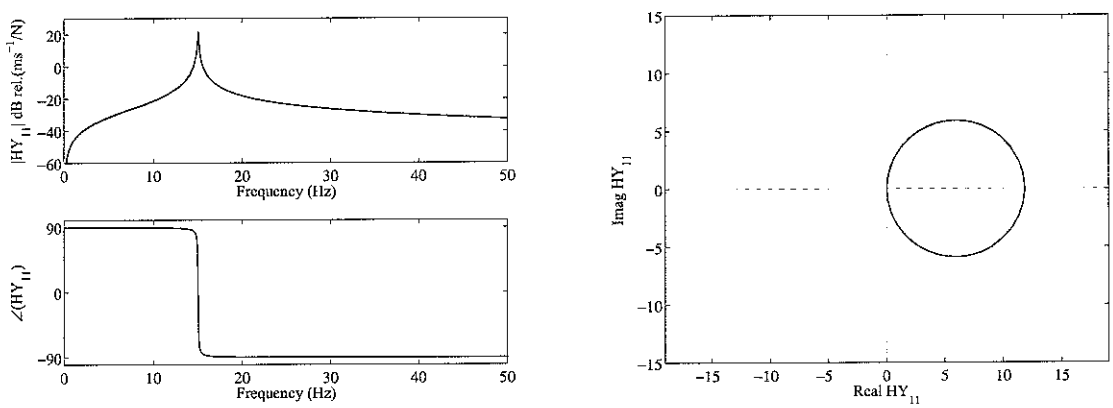

Figure 5: *Frequency response functions; amplitude (top left), phase (bottom left) and Nyquist plot (right) of the open loop sensor–actuator frequency response function in the frequency range between 0-50 Hz when a Proportional control is used.*

The phase plot confirms that the frequency response function HY_{11} of the SDOF active system is positive real so that the system is unconditionally stable. Alternatively the Nyquist plot of HY_{11} in Figure 5 (right plot) shows that the polar plot of the frequency

response function is entirely on the right hand side quadrants and thus it is positive real, which also indicates the unconditional stability of proportional, that is negative velocity feedback, control.

§ Integral Control. Displacement Feedback.

In order to implement negative displacement feedback, the output signal from the velocity sensor is feedback to the actuator via a negative integral control function; $H(\omega)=-g/j\omega$, and thus:

$$F_c = -\frac{g}{j\omega}\dot{X}_1 \,, \tag{2.23}$$

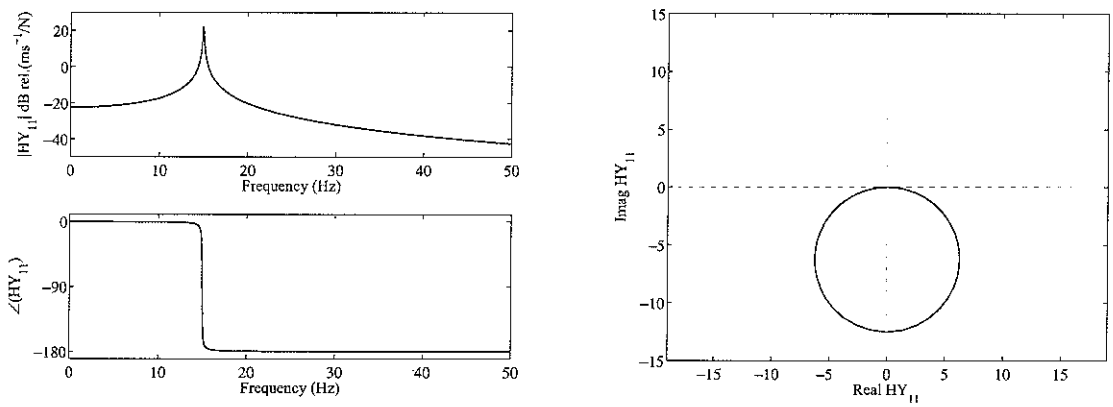

Figure 6: *Frequency response functions; amplitude (top left), phase (bottom left) and Nyquist plot (right) of the open loop sensor–actuator frequency response function in the frequency range between 0-50 Hz when an Integral control is used.*

As shown in Figure 6, in this case the phase plot indicates that the phase of the open loop sensor–actuator frequency response function HY_{11} exceed –90° at higher frequencies above resonance. Therefore the Nyquist plot of HY_{11} is not confined on the right hand side quadrants which suggests that the system could be unstable. Indeed the Nyquist plot of HY_{11} in Figure 6 is characterised by a circle which occupies the bottom quadrants only. Thus in principle, the system is unconditionally stable although part of the circle is very close to the Nyquist instability point $(-1+j0)$ and thus it is likely to intersect the negative real axis at higher frequencies even with little variations of the response function which can be easily generated by external factors that would cause the system to become unstable. Also, when the polar plot of HY_{11} enters

the circle of unit radius and centre $(-1,j0)$, but does not encircle the instability point $(-1,j0)$, then $\mathrm{Re}\{1/(1+HY_{11})\}>1$ and thus, according to Eq. (2.21), even though the system is not unstable, the response $\dot{X}_1$ is magnified rather than minimised. This phenomenon is known as control spillover. In this report the circle of unit radius and centre $-1, j0$, will be referred as the "spillover circle".

§ Derivative Control. Acceleration Feedback.

In order to implement negative acceleration feedback the output signal from the velocity sensor is feedback to the actuator via a negative derivative control function; $H(\omega)=-gj\omega$ and thus:

$$F_c = -j\omega g\dot{X}_1 \ , \tag{2.24}$$

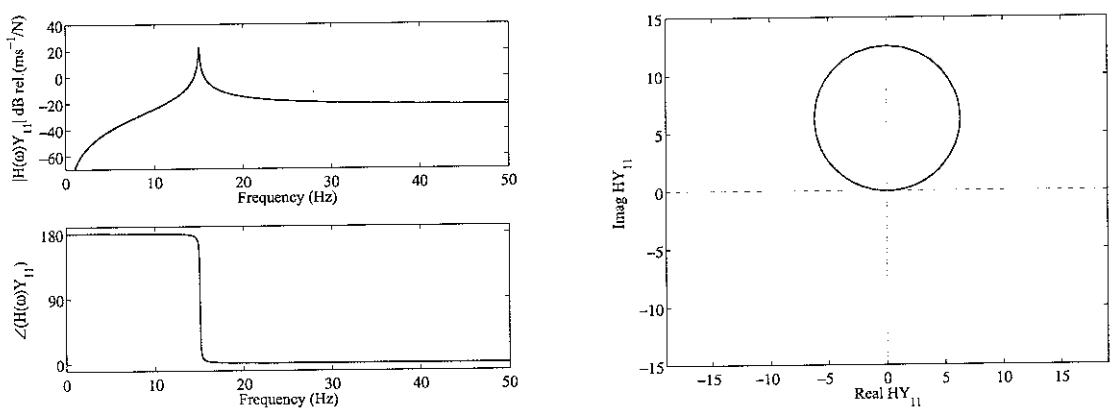

Figure 7: *Frequency response functions; amplitude (top left), phase (bottom left) and Nyquist plot (right) of the open loop sensor–actuator frequency response function in the frequency range between 0-50 Hz when a Derivative control is used.*

As shown in Figure 7 in this case the phase plot indicates that the phase of the open loop sensor–actuator frequency response function HY_{11} exceed + 90° at lower frequencies below resonance. Therefore the Nyquist plot of HY_{11} is not confined on the right hand side quadrants which suggests that the system could be unstable. Indeed the Nyquist plot of HY_{11} in Figure 7 is characterised by a circle which occupies the top quadrants only. Thus in principle, the system is unconditionally stable although part of the circle is very close to the Nyquist instability point $(-1+j0)$ and thus it is likely to intersect the negative real axis at lower frequencies when the response function is modified by the presence of external factors that bring the system to instability. In this

case, the polar plot enters the spillover circle at low frequencies where control spill-over vibration enhancement effects will therefore be generated for high control gains.

§ PID Control.

In order to implement a combination of negative displacement velocity and acceleration feedback, the output signal from the velocity control sensor is feedback to the control force actuator via a negative combination of Proportional–Integral–Derivative functions;$H(\omega) = -g\{ k_P + k_I/j\omega + j\omega k_D\}$ and thus:

$$F_c = -g\left\{k_P + \frac{k_I}{j\omega} + j\omega k_D\right\}\dot{X}_1, \tag{2.25}$$

where k_P, k_I and k_D are Proportional, Integral and Derivative Control constants respectively and their values are summarized in Table 2.

Table 2: *Physical parameters for the Proportional, Integral and Derivative Control constants.*

Parameter	Value
Proportional Control Constant	$k_P = 0.1$
Integral Control Constant	$k_I = 10$
Derivative Control Constant	$k_D = 0.001126$

These Integral and Derivative Control constants have been chosen in such a way that the resonance frequency of the system is kept the same than with no control. The undamped resonance frequency of the PID controlled system can be found by setting to zero the denominator in Eq. (2.16) assuming the complex term due to passive and active damping to be zero:

$$k_1 + k_I - (m_1 + k_D)\omega_n^2 = 0 \ . \tag{2.26}$$

The undamped resonance frequency of the PID active system is therefore given by:

$$\omega_n = \sqrt{\frac{k_1 + k_I}{m_1 + k_D}} \ . \tag{2.27}$$

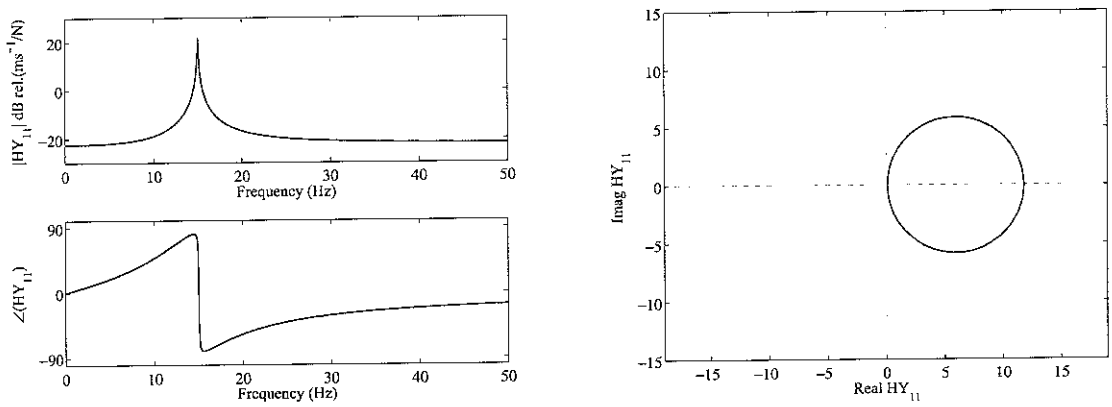

Figure 8: *Frequency response functions; amplitude (top left), phase (bottom left) and Nyquist plot (right) of the open loop sensor–actuator frequency response function in the frequency range between 0-50 Hz when a PID control is used.*

In this case the phase plot in Figure 8 indicates that the phase of the open loop sensor–actuator frequency response function HY_{11} is positive real. Alternatively the Nyquist plot in Figure 8 (right plot) and Figure 9 show that the open loop response function HY_{11} is entirely on the right hand side quadrants, which also indicates the unconditional stability of the system. This is due to the fact that the system adds the same percentage of Integral control (Active stiffness) and Derivative control (Active mass); so that their phase lag and phase lead effects are balanced.

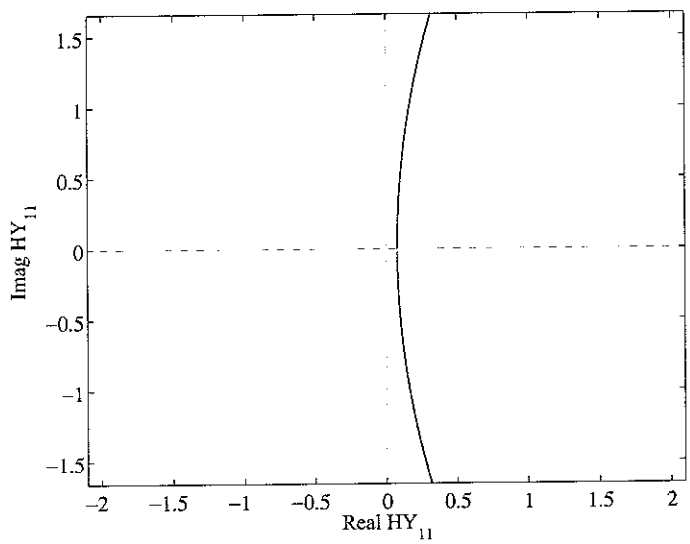

Figure 9: *Zoom of the Nyquist plot shows in Figure 8.*

In general it can be concluded that if the Integral and Derivative Control gains are chosen in such a way as to maintain the same resonance frequency of the system, then the Nyquist plot of the open loop sensor–actuator frequency response function HY_{11} will be characterised by a circle in the right hand side quadrants as in the case of no control.

2.4 Control Performances.

In this sub–section the control performances for the different control architectures introduced above will be studied. In the following points the ratio between the velocity of the mass and the base

$$\frac{\dot{X}_1}{Y} = \frac{Y_{12}}{1 + gH(\omega)Y_{11}} \tag{2.28}$$

will be plotted using the different control function $H(\omega)$.

§ Proportional Control.

In this case the control function utilized is a Proportional function; $H(\omega) = -g$. Figure 10 shows that the addition of small amounts of control gain lead to consistent reduction of the response at, or near, resonance without producing any harm at higher frequencies. Also the phase transition is smoothened out.

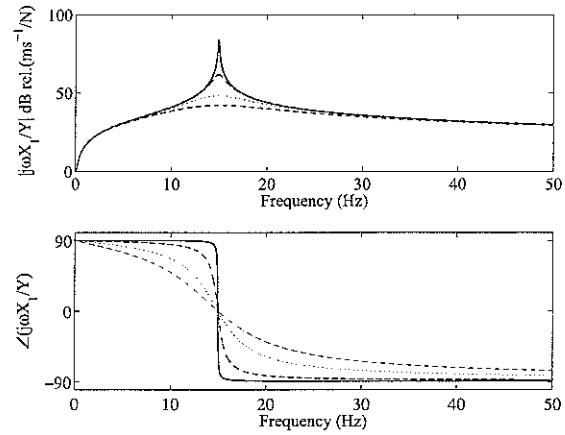

Figure 10: *Modulus and phase of the ratio between the velocity of the inertial mass and displacement of the base of the system shown in Figure 3(a) when the system has a small damping ratio (ξ=0.001) and different values of gain; g_1=0; no-gain (solid line), g_2=0.1 (dashed line), g_3=0.5 (dotted line) or g_4=1 (dash-dot line) when a Proportional control is used.*

In summary, Proportional Control adds active damping such that vibrations reductions are generated at resonances frequencies without side effects below and above resonance frequencies.

§ Integral Control.

In this case the control function is an Integral function; $H(\omega) = -\frac{g}{j\omega}$.

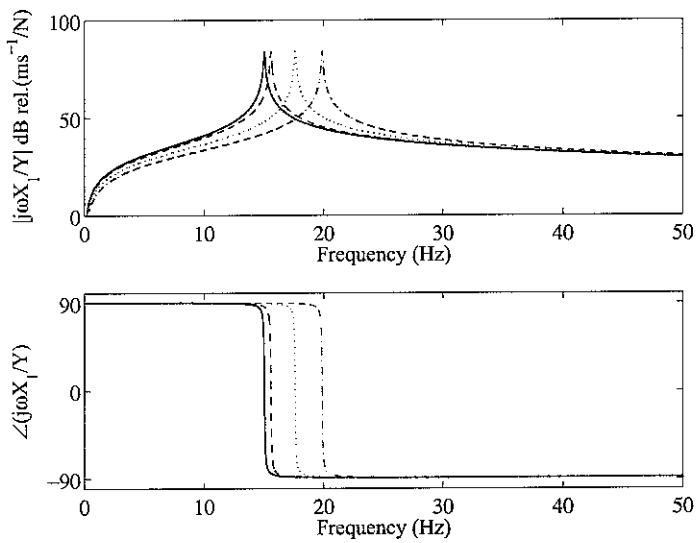

Figure 11: *Modulus and phase of the ratio between the velocity of the inertial mass and the displacement of the base of the system shown in Figure 3(a) when the system has a small damping ratio (ξ=0.001) and different values of gain; g_1=0; no-gain (solid line), g_2=10 (dashed line), g_3=50 (dotted line) or g_4=100 (dash-dot line) when an Integral control is used.*

Figure 11 shows that using Integral control the system adds active stiffness moving the resonance frequency to higher values. Thus the system produces vibration reductions at low frequencies below resonance only. The increase of the resonance frequency can be interpreted as a result of the control spillover effect discussed in section 2.3, which is confirmed by the Nyquist plot in Figure 6 which shows that part of the Nyquist plot of the open loop sensor–actuator response function enters the spillover circle of centre $-1+j0$ and radius 1.

§ Derivative Control.

In this case the control function is a Derivative function given by $H(\omega) = -j\omega g$.

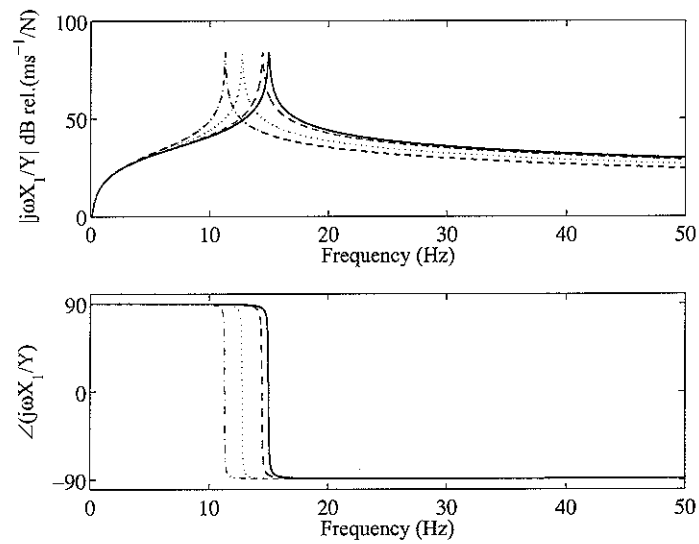

Figure 12: *Modulus and phase of the ratio between the velocity of the inertial mass and the displacement of the base of the system shown in Figure 3(a) when the system has a small damping ratio (ξ=0.001) and different values of gain; g_1=0; no-gain (solid line), g_2=0.001 (dashed line), g_3=0.005 (dotted line) or g_4=0.01 (dash-dot line) when a Derivative control is used.*

Figure 12 shows that using Derivative control the system adds active mass moving the resonance frequency to lower values. Thus the system produces vibration reductions at high frequencies above resonance only. Also in this case the lowering of the resonance frequency can be interpreted as a control spillover effect as suggested by the Nyquist plot in Figure 7 which shows that the low frequency part of the Nyquist plot of the open loop sensor–actuator response function enter the spillover circle of centre $-1+j0$ and radius 1.

§ PID Control.

In this case the control function used is a combination of Proportional–Integral–Derivative function $H(\omega)=-g\left\{k_P+\frac{k_I}{j\omega}+j\omega k_D\right\}$.

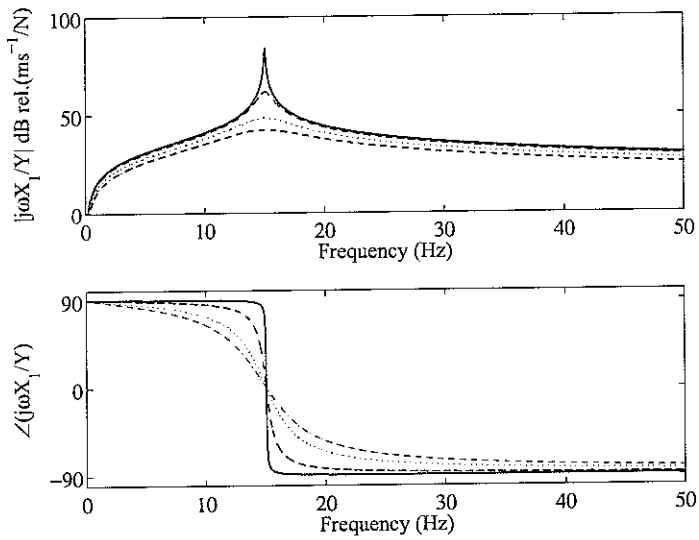

Figure 13: *Modulus and phase of the ratio between the velocity of the inertial mass and the displacement of the base of the system shown in Figure 3(a) when the system has a small damping ratio (ξ=0.001) and different values of gain; g_{k1}=0, g_{c1}=0, g_{m1}=0; no-gain (solid line), g_{k2}=10, g_{c2}=0.1, g_{m2}=0.001; (dashed line), g_{k3}=50, g_{c3}=0.5, g_{m3}=0.005 (dotted line) or g_{k4}=100, g_{c4}=1, g_{m4}=0.01 (dash-dot line) when a PID control is used.*

As it was seen in previous sections; a) Proportional Control reduces vibration at resonance, b) Integral Control reduces the vibration at low frequency below resonance and c) Derivative Control reduces the vibration at high frequency above resonance. Therefore, as shown in Figure 13, using a combination among the three will reduce the vibration in the three regions.

3. FEEDBACK CONTROL ON A SDOF SYSTEM WITH INERTIAL ACTUATOR.

In this section, the dynamic response of a two degree of freedom system will be considered. The aim of this study is to introduce the analysis of vibration control using inertial actuators. Therefore, considering the drawing in Figure 14, the bottom mass–spring–dashpot elements represent the system to be controlled which is excited by the force f_1. The inertial actuator is composed by an additional mass–spring–dashpot system placed on top of the system to be controlled, so that, as will be shown in section 3.2, a control force is generated on the mass m_1 by reacting on the mass m_2. The form of this excitation will be $f_1(t) = \mathrm{Re}\{F_1(\omega)e^{j\omega t}\}$, where $F(\omega)$ is the complex amplitude. The response of this system will be studied first when there is no feedback active vibration control and then when various types of feedback control functions are implemented.

As in the previous chapter different Control architectures will be studied; a) Proportional Control for implementation of Velocity Feedback, b) Integral Control for implementation of Displacement Feedback c) Derivative Control for implementation of Acceleration Feedback d) PID Control (Proportional-Integral-Derivative Feedback Control) e) PI Control (Proportional-Integral Feedback Control) and f) PD Control (Proportional-Derivative Feedback Control).

3.1 Two DOF under harmonic force when there is no control feedback.

Figure 14(a) shows the notation used for the mass–spring–dashpot two DOF system considered in this chapter.

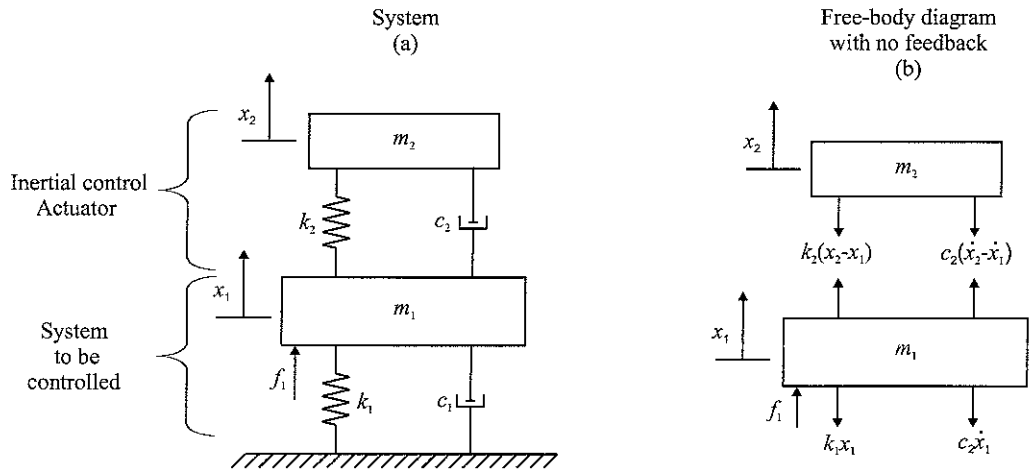

Figure 14: *Two DOF system under harmonic force when Fc=0.*

Considering the free–body diagram with F_c=0 shown in Figure 14(b) above and using Newton's second law of motion to each of the masses gives the equations of motion:

$$\begin{cases} m_1\ddot{x}_1 + (c_1 + c_2)\dot{x}_1 - c_2\dot{x}_2 + (k_1 + k_2)x_1 - k_2x_2 = f_1 \\ m_2\ddot{x}_2 - c_2\dot{x}_1 + c_2\dot{x}_2 - k_2x_1 + k_2x_2 = 0 \end{cases}. \tag{3.1}$$

Eq. (3.1) can be written in matrix form as:

$$\mathbf{M}\ddot{\mathbf{x}} + \mathbf{C}\dot{\mathbf{x}} + \mathbf{K}\mathbf{x} = \mathbf{h}_1 f_1 \ , \tag{3.2}$$

where:

$$\mathbf{M} = \begin{pmatrix} m_1 & 0 \\ 0 & m_2 \end{pmatrix}, \tag{3.3}$$

$$\mathbf{C} = \begin{pmatrix} c_1 + c_2 & -c_2 \\ -c_2 & c_2 \end{pmatrix}, \tag{3.4}$$

$$\mathbf{K} = \begin{pmatrix} k_1 + k_2 & -k_2 \\ -k_2 & k_2 \end{pmatrix}, \tag{3.5}$$

$$\mathbf{h}_1 = \begin{pmatrix} 1 \\ 0 \end{pmatrix}, \tag{3.6}$$

$$\ddot{\mathbf{x}} = \begin{pmatrix} \ddot{x}_1 \\ \ddot{x}_2 \end{pmatrix}, \quad \dot{\mathbf{x}} = \begin{pmatrix} \dot{x}_1 \\ \dot{x}_2 \end{pmatrix} \text{ and } \quad \mathbf{x} = \begin{pmatrix} x_1 \\ x_2 \end{pmatrix}. \tag{3.7}$$

The steady state solution of Eq. (3.2) can be found by assuming:

$$\mathbf{x}(t) = \mathrm{Re}\left\{ \mathbf{X}e^{j\omega t} \right\}, \tag{3.8}$$

where:

$$\mathbf{X} = \begin{Bmatrix} X_1 \\ X_2 \end{Bmatrix}. \tag{3.9}$$

By substituting Eq. (3.8) into Eq. (3.2), and solving for **X**, the following expression is obtained:

$$\mathbf{X}(\omega) = \left\{-\omega\mathbf{M} + j\omega\ \mathbf{C} + \mathbf{K}\right\}^{-1} \cdot \mathbf{h}_1 F_1, \tag{3.10}$$

Table 3: *Physical parameters for the elements in the SDOF system.*

Parameter	Value
Resonance frequency of the structure to be controlled	$f_{n1} = 40$ Hz
Resonance frequency of inertial actuator	$f_{n2} = 15$ Hz
Mass of Structure to be controlled	$m_1 = 0.350$ Kg
Mass of the Inertial actuator	$m_2 = 0.030$ Kg
Stiffness of the structure to be controlled	$k_1 = 2.21\ 10^4$ N/m
Stiffness of the inertial actuator	$k_2 = 266.5$ N/m
Critical Damping of the structure to be controlled	$c_{c1} = 175.9$ N/ms^{-1}
Critical Damping of inertial actuator	$c_{c2} = 5.65$ N/ms^{-1}
Damping ratio of the structure to be controlled	$\zeta_1 = 0.01$
Damping ratio of the inertial actuator	$\zeta_2 = 0.1$

The physical parameters used in the simulation study presented in this chapter are summarized in Table 3.

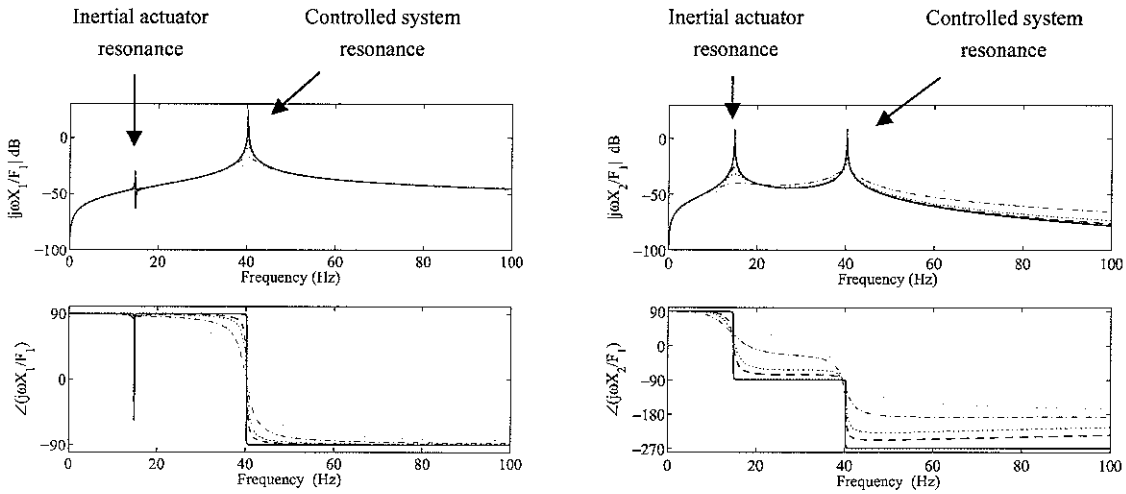

Figure 15: *Modulus and phase of the velocities of the system to be controlled (m_1) (left plots) and the inertial actuator (m_2) (right plots) of the system shown in Figure 14(a) when there is no active vibration control considering different values of damping ratio; ξ_1=0.001 (solid line), ξ_2=0.03 (dashed line), ξ_3=0.06 (dotted line), ξ_4=0.1 (dash-dot line) or ξ_5=0.3 (dotted line).*

The mass and stiffness of the actuator has been chosen much smaller compared to that of the system to be controlled. In order to obtain the maximum vibration reduction

and stability in the resonance of the system to be controlled, the natural frequency of the resonance of the actuator must be lower than the natural frequency of resonance of the system to be controlled [5]. Therefore the mass/stiffness ratio of the actuator should be selected in such a way as to keep the natural frequency of the actuator lower than frequency of the system to be controlled. As shown in Figure 15, the first resonance, at about 15 Hz, is primarily a control actuator resonance since $X_2>X_1$. The second resonance, at about 40 Hz, is mainly linked to the response of the base system to be controlled since $X_1>X_2$. As seen for the SDOF problem, when damping level in the system to be controlled, c_1, is increased then the response at its fundamental resonance frequency at about 40 Hz goes down although in this case there is no degrading effect at higher frequencies as was noted for the base vibration SDOF problem considered above.

3.2 Two DOF under harmonic force with Feedback Control.

A valuable way to enhance the vibration isolation of the structure to be controlled is the implementation of active control. In this section the effects produced by a feedback control system, which, as shown in Figure 16(a), is composed by a) a control sensor that measures the velocity of the mass of the system to be controlled; m_1, b) the inertial actuator composed by the top spring–dashpot–mass system and c) a control system that implement a control function $H(\omega)$.

As done in the previous chapter, different Control architectures will be studied; a) Proportional Control, b) Integral Control, c) Derivative Control, d) PID Control (Proportional–Integral–Derivative Feedback Control), e) PI Control (Proportional–Integral Feedback Control) and f) PD Control (Proportional–Derivative Feedback Control).

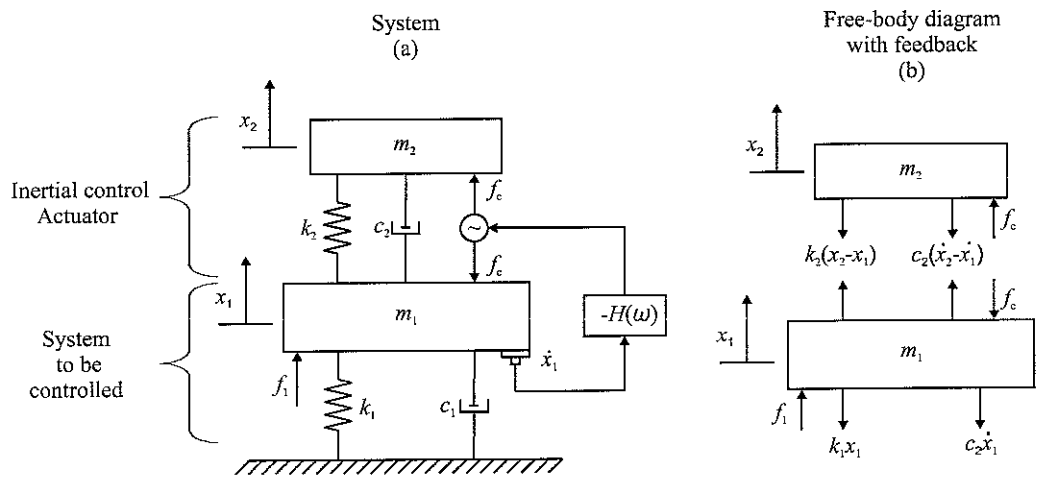

Figure 16: *Two DOF under harmonic force with feedback.*

In this case the response of the active system shown in Figure 16 will only be formulated in terms of mobility frequency response functions.

3.3 Stability analysis.

As done in section 2.3, the stability of the feedback control loop will be assessed in view of the Nyquist criterion considering the Bode and Nyquist plots of the open loop HY_{11} sensor–actuator frequency response function.

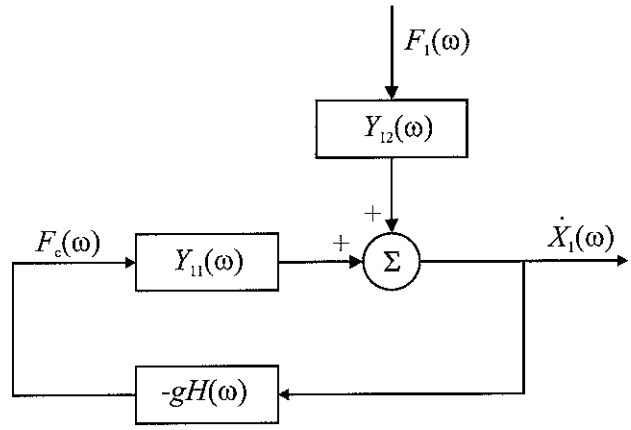

Figure 17: *Block diagram of Feedback Control implemented on the Two DOF system.*

Following the same procedure as in section 2.3, the response of the system shown in Figure 16 can be formulated in terms of mobility functions. From Figure 17 the following expression for $\dot{X}_1$ and control force F_c are obtained:

$$\dot{X}_1 = Y_{12}F_1 + Y_{11}F_c \ , \tag{3.11}$$

$$F_c = -gH(\omega)\dot{X}_1 \ , \tag{3.12}$$

where the mobility functions Y_{21} and Y_{22} are given by:

$$Y_{12} = \left.\frac{\dot{X}_1}{F_1}\right|_{F_c=0} = j\omega \lfloor 1 \quad 0 \rfloor \left(\{-\omega\mathbf{M} + j\omega\mathbf{C} + \mathbf{K}\}^{-1} \cdot \mathbf{F} \right) \ , \tag{3.13}$$

$$Y_{11} = \left.\frac{\dot{X}_1}{F_c}\right|_{F_1=0} = j\omega \lfloor 1 \quad 0 \rfloor \left(\{-\omega\mathbf{M} + j\omega\mathbf{C} + \mathbf{K}\}^{-1} \cdot \begin{Bmatrix} -1 \\ 1 \end{Bmatrix} \right) \ , \tag{3.14}$$

where **F** is the excitation force vector defined by:

$$\mathbf{F} = \begin{Bmatrix} F_1 \\ 0 \end{Bmatrix} . \tag{3.15}$$

The open loop sensor–actuator frequency response function HY_{11} depends on the specific control function H implemented in the feedback loop. The stability of the different control functions will be studied in the following points. Substituting Eq. (3.12) into Eq. (3.11), and solving respect to the velocity of the mass to be controlled (m_1), the following expression is obtained:

$$\dot{X}_1 = \frac{Y_{12}}{1 + gHY_{11}} F_1 , \tag{3.16}$$

where HY_{11} is the open loop frequency response function between the velocity sensor on the mass of the system to be controlled (m_1) and the control force. As anticipated in the previous chapter if $\mathrm{Re}(HY_{11})>0$, then Eq. (3.16) shows that $\dot{X}_1 / F_1 < 1$ for any control gain and frequency, that is the feedback control decrease the velocity of the base system for any control gain and frequency.

§ Proportional Control.

In order to implement negative velocity feedback, the output signal from the velocity control sensor on the mass of the structure to be controlled (m_1) is feedback to the actuator via a negative Proportional control function $H(\omega)=-g$, and thus:

$$F_c = -g\dot{X}_1 . \tag{3.17}$$

Figure 18 shows the amplitude–phase and Nyquist plots of the open loop sensor–actuator frequency response function HY_{11} in the frequency range between 0 and 100 Hz.

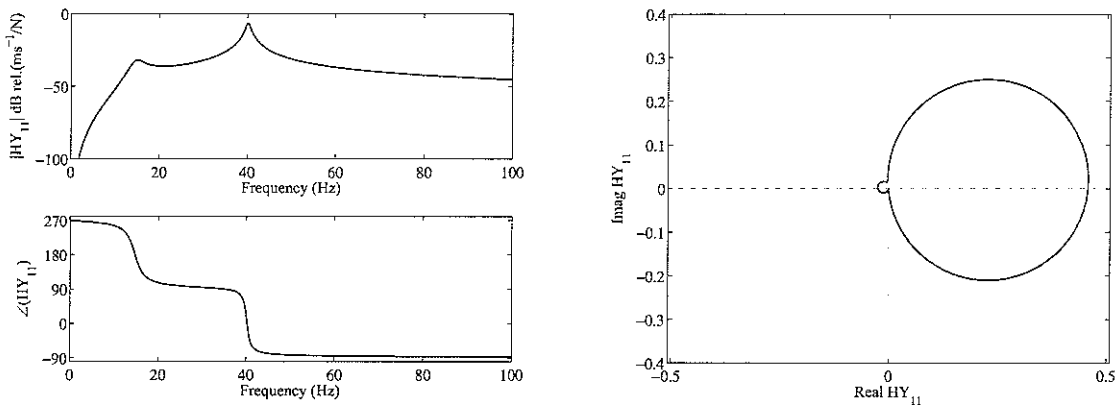

Figure 18: *Frequency response functions; amplitude (top left), phase (bottom left) and Nyquist plot (right) of the open loop sensor–actuator frequency response function in the frequency range between 0-100 Hz when a Proportional control is used.*

In this case the phase plot indicates that the phase of the open loop sensor–actuator frequency response function starts from +270°, drops to +90° after the first resonance of the actuator and then goes to –90° after the resonance of the system to be controlled. Therefore the Nyquist plot shows two circles (one for each resonance); the left hand side circle is "controlled" by the resonance of the actuator and the right hand side circle is "controlled" by the resonance of the mass of the system to be controlled. The actuator circle is confined on the left hand side quadrants which suggest that the system is unstable. Indeed the Nyquist plot in Figure 18 indicates that for large control gains the Nyquist instability point ($-1+j0$) can be encircled, so that, the control system goes unstable.

§ Integral Control.

In order to implement negative displacement feedback, the output signal from the velocity control sensor on the mass to be controlled (m_1) is feedback to the actuator via a negative Integral control function $H(\omega)=-g/j\omega$, and thus:

$$F_c = -\frac{g}{j\omega}\dot{X}_1 \,. \tag{3.18}$$

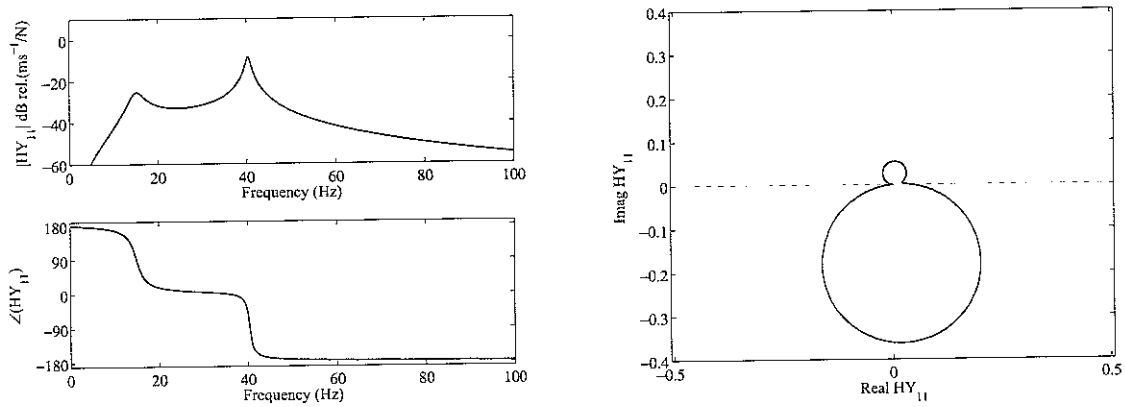

Figure 19: *Frequency response functions; amplitude (top left), phase (bottom left) and Nyquist plot (right) of the open loop sensor–actuator frequency response function in the frequency range between 0-100 Hz when an Integral control is used.*

In this case the phase plot indicates that the phase of the open loop sensor–actuator frequency response function exceed +90° at lower frequencies below the resonance of the inertial actuator and –90° at higher frequencies above the resonance of the mass to be controlled. This is due to the fact that with Integral Control the system adds –90° phase lag to the open loop sensor–actuator response function of the Proportional control system.

Therefore the Nyquist plot shows two circles one on the top side quadrants, which is due to the actuator–resonance, and the other on the bottom side quadrants, which is due to the resonance of the system to be controlled, which suggest that the control system could go unstable, both at low and high frequency. In fact part of the circles are very close to the Nyquist instability point ($-1+j0$) and thus even with little variations of the response function which can be easily generated by external factors the system can become unstable. Besides, the two circles enter the spillover circle so that the control spillover effects are likely to happen at low and high frequencies when the high control gains are implemented. The larger size of the lower loop suggests that the spillover effect associated to the second resonance, and thus at higher frequencies, is likely to be more effective.

§ Derivative Control.

In order to implement negative acceleration feedback, the output signal from the velocity control sensor on the mass to be controlled (m_1) is feedback to the actuator via a negative Derivative control function $H(\omega)=-gj\omega$, and thus:

$$F_c = -j\omega\dot{X}_1 \ . \tag{3.19}$$

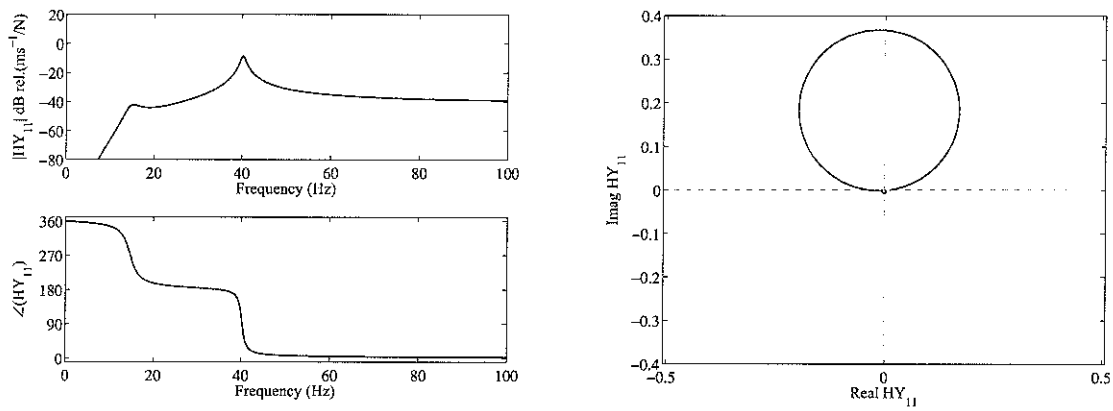

Figure 20: *Frequency response functions; amplitude (top left), phase (bottom left) and Nyquist plot (right) of the open loop sensor–actuator frequency response function in the frequency range between 0-100 Hz when a Derivative control is used.*

In this case the phase plot indicates that the phase of the open loop sensor–actuator frequency response function is about +360° at lower frequencies below the resonance frequency of the resonance frequency of the actuator. This is due to the fact that with Derivative Control the system adds +90° phase lead to the Proportional system.

Therefore the Nyquist plot shows two circles one on the top side quadrants due to the SDOF system to be controlled and another much smaller on the bottom side quadrants due to the inertial actuator which suggest that the system could be unstable. According to the plot in Figure 20, the system should be unconditionally stable although part of the circles are very close to the Nyquist instability point ($-1+j0$) and thus the closed loop is likely to become unstable even with little variations of the response function which can be easily generated by external factors. Similarly to the previous control case, control spillover is likely to happen both at low and higher frequencies although, as seen for the integral control the larger size of the top circle indicates that the bigger spillover effect occurs at higher frequencies.

§ PID Control.

In order to implement a combination of negative displacement velocity and acceleration feedback control, the output signal from the velocity sensor in the mass to be controlled (m_1) is feedback to the control force actuator via a negative mix of Proportional–Integral–Derivative control function $H(\omega)= -g\{ k_P + k_I/j\omega + j\omega k_D\}$ and thus:

$$F_c = -g\left\{k_P + \frac{k_I}{j\omega} + j\omega k_D\right\}\dot{X}_1, \tag{3.20}$$

where k_P, k_I and k_D are Proportional, Integral and Derivative Control constants respectively and their values are summarized in Table 4. Figure 21 shows this control function.

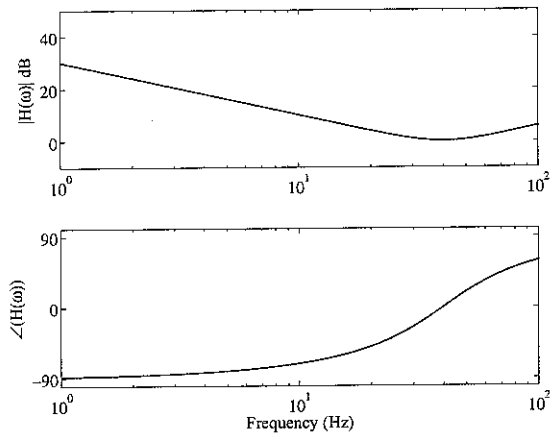

Figure 21: *Control function when a PID Control is used.*

Figure 21 shows that a) at the second resonance $H(\omega)$ is a proportional function controls the response; b) below the second resonance $H(\omega)$ is an integral function, and c) above resonance the second resonance $H(\omega)$ is a derivative function.

Table 4: *Physical parameters for the Proportional, Integral and Derivative Control constants used in the two DOF system.*

Parameter	Value
Proportional Control Constant	$k_P = 1$
Integral Control Constant	$k_I = 1000$
Derivative Control Constant	$k_D = 0.01583$

The Integral and Derivative Control constants have been chosen in such a way to maintain constant the undamped resonance frequency of the system to be controlled.

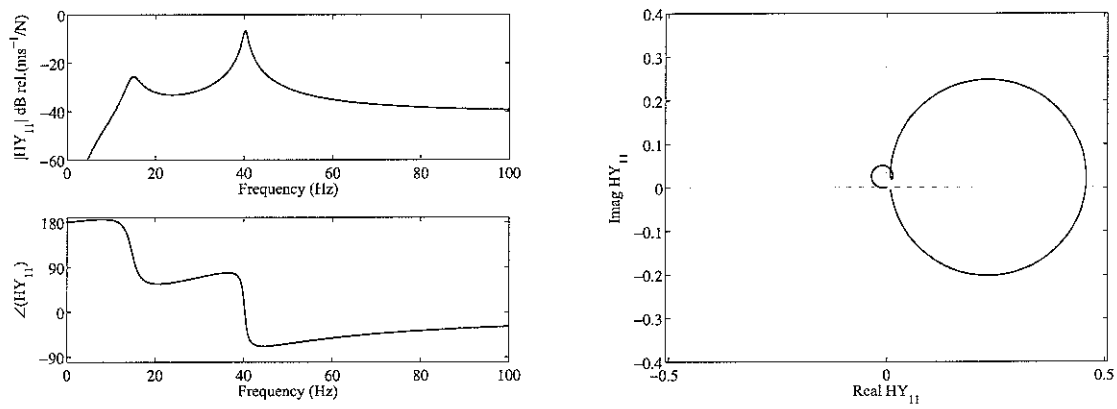

Figure 22: *Frequency response functions; amplitude (top left) and phase (bottom left). Nyquist plot (right plot) for the frequency response functions between a collocated ideal velocity sensor in the mass to be controlled (m_1) and force actuator in the 0-100 Hz frequency range in a two DOF when a PID Control is used.*

The Bode plot in Figure 22 shows that the phase of the open loop response is about 180° below the first resonance of the actuator, it then goes down to about 0° and rises to +45° at about the second resonance linked to the system to be controlled. Finally it moves down to –45° above this resonance and it gradually moves back to 0° as the frequency rises.

Therefore the Nyquist plot in Figure 22 shows two circles one on the right hand side quadrants due to the system to be controlled and other much smaller on the top side quadrants due to the inertial actuator which suggest that the system could be unstable at low frequencies. Indeed the zoom of the Nyquist plot shown in Figure 23 indicates that the sensor–actuator response function can became close to the instability point $(-1+j0)$ at low frequency when large control gains are implemented.

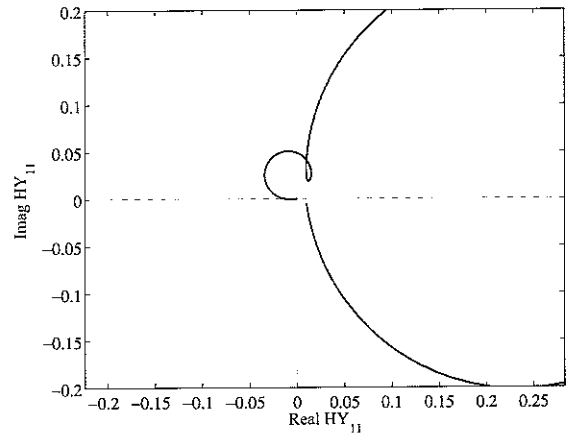

Figure 23: *Zoom Nyquist plot shows in Figure 22.*

In order to keep the same resonance frequency of the base system, the proportional k_I and derivative k_D constants have been chosen in such a way to satisfy the following relation:

$$\omega_n^{\,2} = \frac{1}{2}\left\{\frac{((k_1+k_I)+k_2)m_2+k_2(m_1+k_D)}{(m_1+k_D)m_2}\right\} + \frac{1}{2}\sqrt{\left\{\frac{((k_1+k_I)+k_2)m_2+k_2(m_1+k_D)}{(m_1+k_D)m_2}\right\}^2 - 4\left\{\frac{((k_1+k_I)+k_2)k_2-k_2^{\,2}}{(m_1+k_D)m_2}\right\}}, \quad (3.21)$$

where ω_n is the second natural frequency which is primarily linked to the vibration of the base system. As a result, the integral constant k_I is much higher than the derivative constant k_D so that the derivative control effect at higher frequencies is likely to be more effective than the integral control at lower frequencies.

§ PI Control.

In order to implement a combination of negative velocity and displacement feedback the output signal from the velocity control sensor in the mass to be controlled (m_1) is feedback to the control force actuator via a negative combination of Proportional–Integral control function $H(\omega) = -g\{ k_P + k_I/j\omega\}$ and thus:

$$F_c = -g\left\{k_P + \frac{k_I}{j\omega}\right\}\dot{X}_1 \,, \tag{3.22}$$

where k_P and k_I are Proportional and Integral constants respectively and their values are summarized in Table 4. Figure 24 shows the control function.

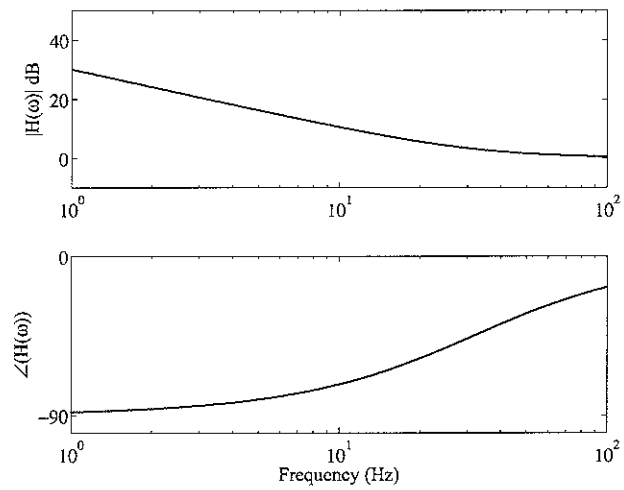

Figure 24: *Control function when a PI Control is used.*

Figure 24 shows that up to approximately 50 Hz the Integral function controls the response which then starts to move towards a Proportional function.

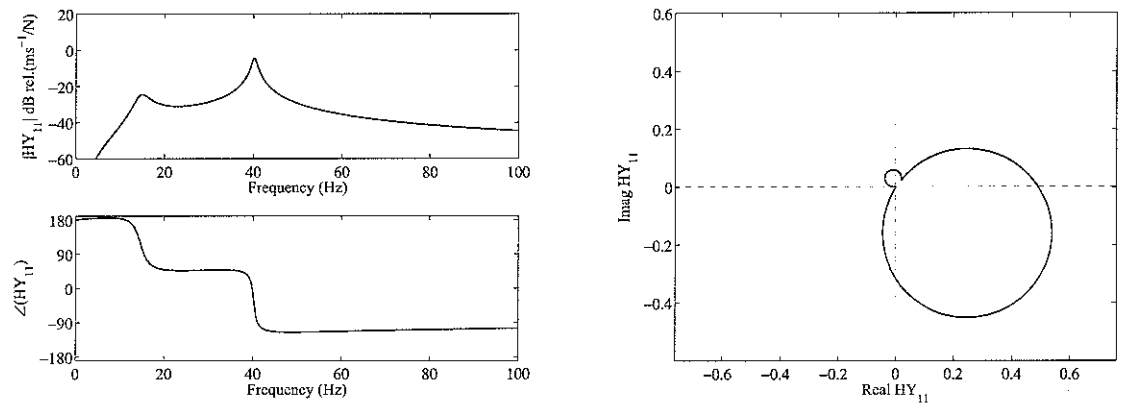

Figure 25: *Frequency response functions; amplitude (top left) and phase (bottom left). Nyquist plot (right plot) for the frequency response functions between a collocated ideal velocity sensor in the mass to be controlled and force actuator in the 0-100 Hz frequency range in a two DOF when a PI Control is used.*

As shown in Figure 25, in this case the phase plot of the open loop response function indicates that the phase of the open loop sensor–actuator frequency response function exceed +90° at lower frequencies below the resonance frequency of the inertial actuator and –90° at higher frequencies above the resonance frequency of the system to be controlled. This is due to the fact that with PI Control the system adds almost –90° phase lag to the open loop frequency response function of the proportional control loop. The Nyquist plot shows two circles one on the top side quadrants due to the actuator resonance and the other on the bottom side quadrants due to the resonance of the system to be controlled. Indeed the Nyquist plot shown in Figure 25 is characterised by two circles where as shown in the zoom of Figure 26 the actuator circle is turned towards the Nyquist instability point (–1+j0).

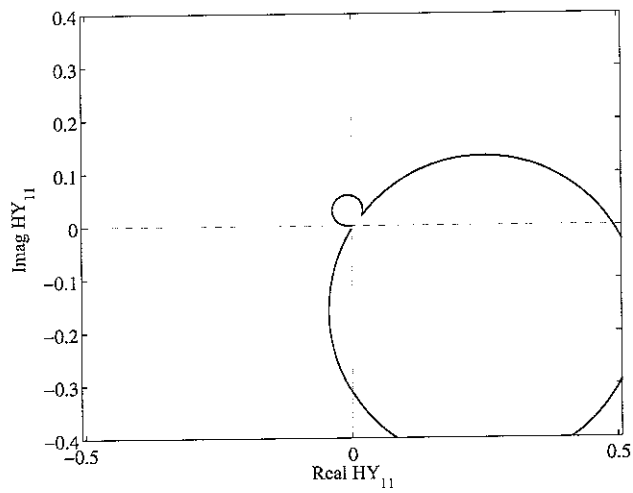

Figure 26: *Zoom Nyquist plot shows in Figure 25.*

§ PD Control.

In order to implement a combination of negative velocity and acceleration feedback the output signal from the velocity control sensor in the mass to be controlled (m_1) is feedback to the control force actuator via a negative combination of Proportional–Derivative control function $H(\omega)=-g\{\ k_P + j\omega k_D\}$ and thus:

$$F_c = -g\{k_P + j\omega k_D\}\dot{X}_1\ , \tag{3.23}$$

where k_P and k_D are Proportional and Derivative Control gains respectively and their values are summarized in Table 4. Figure 27 shows that below about 10 Hz $H(\omega)$ is

proportional function while at higher frequencies above 10 Hz it is a derivative function.

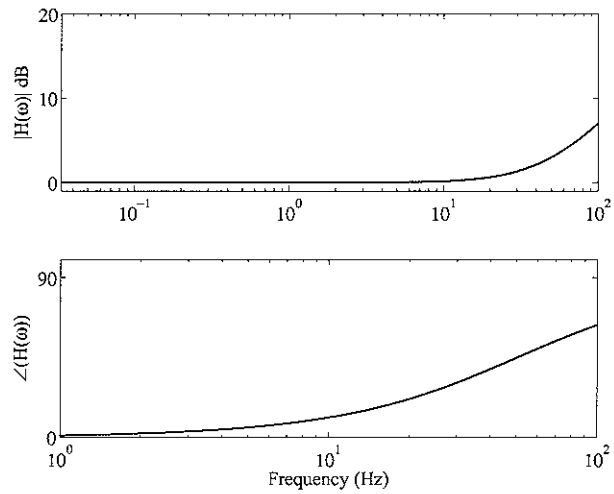

Figure 27: *Control function when a PD Control is used.*

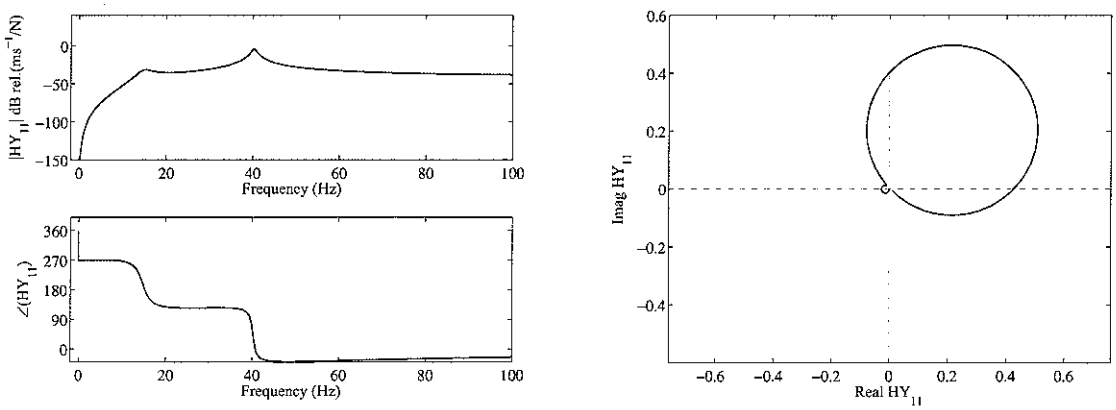

Figure 28: *Frequency response functions; amplitude (top left) and phase (bottom left). Nyquist plot (right plot) for the frequency response functions between a collocated ideal velocity sensor in the mass to be controlled and force actuator in the 0-100 Hz frequency range in a two DOF when a PD Control is used.*

In this case the phase plot in Figure 28 indicates that the phase of the open loop sensor–actuator frequency response function exceed even 180° at lower frequencies below the resonance frequency of the inertial actuator. This is due to the fact that with PD Control the system adds almost +90° phase lead to the open loop sensor–actuator frequency response function of the proportional control.

Therefore as shown in Figure 28 the Nyquist plot show two circles one on the top side quadrants due to the base system to be controlled and the other much more smaller on the bottom side quadrants due to the inertial actuator.

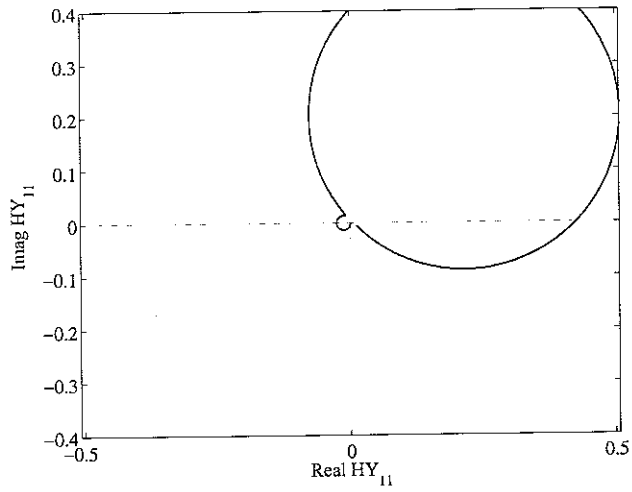

Figure 29: *Zoom Nyquist plot show in Figure 28.*

The zoom in Figure 29, shows that the circle due to the low frequency actuator clearly intersects the real–negative axis which indicates that for too large control gains the system may go unstable.

3.4 Control performances.

In this section the control performances for the various control architectures discussed in the previous section will be studied. In the following points the ratio between the velocity of the mass of the system to be controlled (m_1) and the harmonic force F_1, $\dot{X}_1/F_1 = Y_{12}/(1+gHY_{11})$ will be plotted with reference to the various $H(\omega)$ control function.

§ Proportional Control.

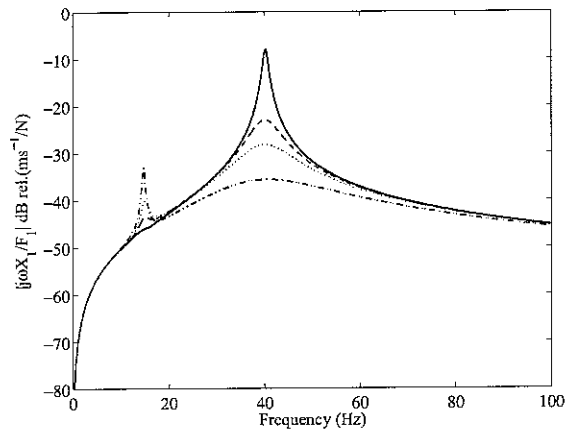

Figure 30: *Modulus of the ratio between velocity of the mass of the system to be controlled and the harmonic force of the system shown in Figure 16(a) when a Proportional Control is used and different values of gain; g_1=0; no-gain (solid line), g_2=10 (dashed line), g_3=50 (dotted line) or g_4=100 (dash-dot line).*

Figure 30 shows the active control effects produced by a proportional control function $H(\omega)=-g$. From this figure it is possible to highlight that the addition of small amounts of control gain lead to large reductions of response at the resonance of the system to be controlled. This is because the control force generated by the inertial actuator produces an active damping effect that, as seen in the previous chapter, tends to reduce the vibration of the base system at resonance frequencies. However it also produces a spillover effect at the inertial actuator resonance as was highlighted by the left hand side circle in the Nyquist plot in Figure 18.

§ Integral Control.

Figure 31 shows the effect of a Integral control function $H(\omega)=-g/j\omega$.

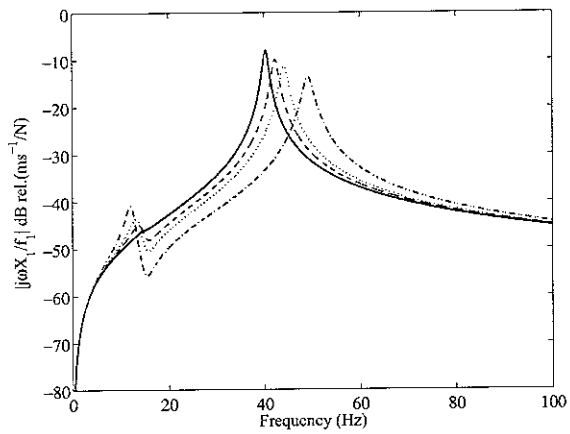

Figure 31: *Modulus of the ratio between velocity of the mass of the system to be controlled and harmonic force of the system shown in Figure 16(a) when a Integral Control is use and different values of gain; g_1=0; no-gain (solid line), g_2=10 (dashed line), g_3=20 (dotted line) or g_4=60 (dash-dot line).*

From this Figure it is possible to highlight that Integral control adds "Active Stiffness" moving the resonance frequency of the system to be controlled to higher values and the resonance frequency of the actuator to lower values. Thus the system produces vibration reductions at low frequencies below the resonance of the system to be controlled, also spillover on the resonance of the actuator is generated as indicated by the Nyquist plot in Figure 19.

§ Derivative Control.

Figure 32 shows the effects generated by a Derivative control function $H(\omega) = -j\omega g$.

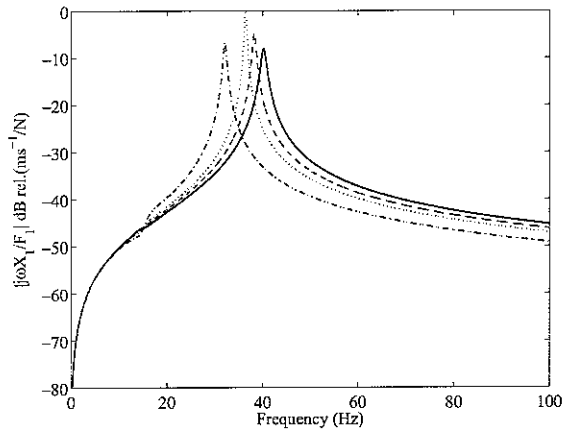

Figure 32: *Modulus of the ratio between velocity of the system to be controlled and harmonic force of the system shown in Figure 16(a) when a Derivative Control is use and different values of gain; g_1=0; no-gain (solid line), g_2=10 (dashed line), g_3=20 (dotted line) or g_4=60 (dash-dot line).*

In this case Derivative Control adds "Active Mass" moving the resonance of the structure to be controlled to lower values, so that vibration reductions are produced at higher frequencies above the resonance of the system to be controlled. Also the resonance frequency of the actuator is moved up so that for high control gain it merges with the resonance of the system to be controlled which is actually falling down under the effect of the active control action.

§ PID Control.

Figure 33 shows the control effects generated by a combination among a Proportional–Integral–Derivative function; $H(\omega) = -g\left\{k_P + \frac{k_I}{j\omega} + j\omega k_D\right\}$:

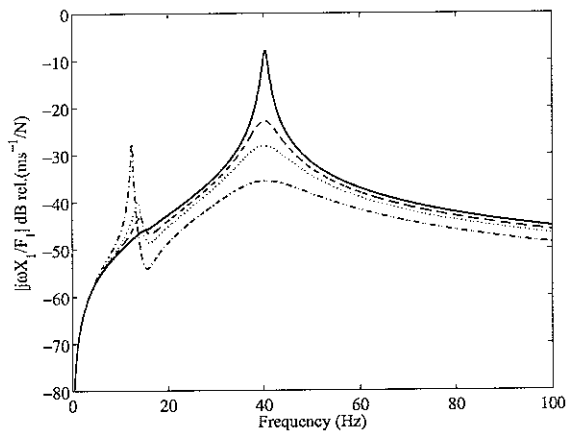

Figure 33: *Modulus of the ratio between velocity of the system to be controlled and the harmonic force of the system shown in Figure 16(a) when a PID Control is use and different values of gain; g_1=0; no-gain (solid line), g_2=10 (dashed line), g_3=20 (dotted line) or g_4=60 (dash-dot line).*

This Figure highlights that PID Control adds: "Active damping", "Active Stiffness" and "Active mass" keeping constant the resonance of the system to be controlled. This system produces vibration reductions in the three regions; below, at and above the resonance of the structure to be controlled. Also, it produces large control spillover effect at the actuator resonance. However the control performance of this loop is limited by stability as it was seen in section 3.3.

§ PI Control.

Figure 34 shows the control effects produced by a combination between Proportional–Integral functions; $H(\omega)=-g\{k_P+k_I/j\omega\}$:

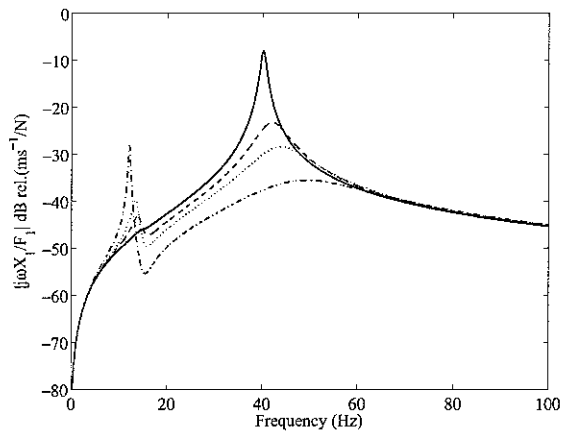

Figure 34: *Modulus of the ratio between velocity of the system to be controlled and harmonic force of the system shown in Figure 16(a) when a PI Control is use and different values of gain; g_1=0; no-gain (solid line), g_2=10 (dashed line), g_3=20 (dotted line) or g_4=60 (dash-dot line).*

This figure highlights that PI Control adds "Active damping" and "Active Stiffness" moving the resonance of the system to be controlled to higher values. This Control moves down the resonance of the actuator and produces spillover due to the Integral Control effect at low frequencies. Thus, the system produces vibration reductions in two regions; below and at resonance of the system to be controlled. However PI control slightly detriment the response above the resonance of the system to be controlled.

§ PD Control.

Figure 35 shows the control effects produced by a combination between a Proportional–Derivative functions; $H(\omega) = -g\{k_P + j\omega k_D\}$:

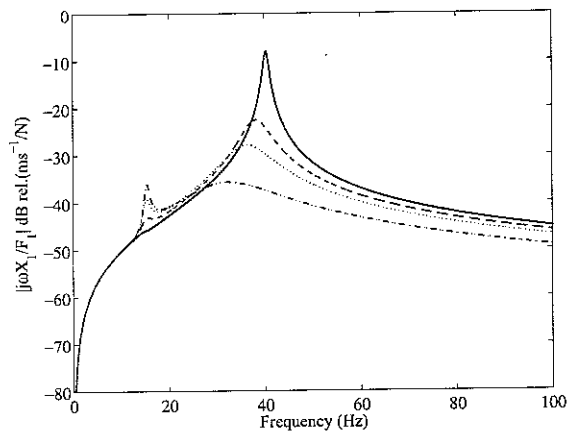

Figure 35: *Modulus of the ratio between velocity of the system to be controlled and harmonic force of the system shown in Figure 16(a) when a PD Control is use and different values of gain; g_1=0; no-gain (solid line), g_2=10 (dashed line), g_3=20 (dotted line) or g_4=60 (dash-dot line).*

This figure highlights that PD Control adds "Active damping" and "Active mass" moving the resonance of the system to be controlled to lower values. Also the resonance of the actuator is moved up, so that for high control gain it merges with the resonance of the system as it was explained above in Derivative Control case. Thus, the system produces vibration reductions in two regions; at and above the resonance of the system to be controlled.

4. FEEDBACK CONTROL IN A PLATE.

In this chapter, the dynamic response of a distributed system such as a plate will be considered. The study is subdivided in six parts. The first part introduce the model for the response of a simple supported plate excited by a primary force with an ideal collocated velocity sensor and point force actuator feedback control system. The second part illustrates the model for the same plate with an inertial force actuator for the feedback control loop. The third and fourth parts show the model for an inertial electro–dynamic actuator mounted on the plate with an ideal collocated velocity sensor at its base for the implementation at either current or voltage control feedback. The fifth and sixth parts discuss the stability and control performances of these systems for the P, I, D and PID different control functions considered in previous chapters.

4.1 Feedback Control with velocity sensor–point force actuator pair.

The system studied in this section consists of a simply supported plate with an ideal collocated velocity sensor and a point force actuator feedback active vibration control system as shown in Figure 36.

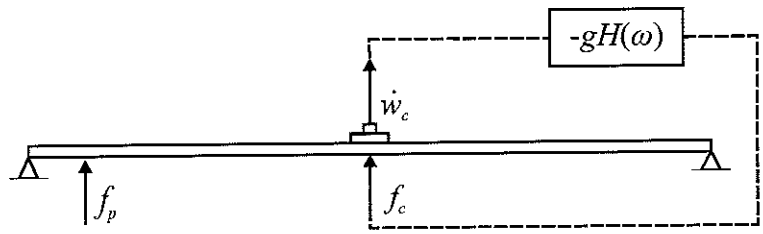

Figure 36: *Simply supported plate excited by a primary force f_p with an ideal collocated velocity sensor and a point force actuator feedback control system.*

The phasor of the transverse velocity on a generic point of the plate structure, $\dot{w}_b(x,y,\omega)$ and at control sensor position, $\dot{w}_c(x_c,y_c,\omega)$, can be expressed in terms of the primary and secondary excitations as follow [10]:

$$\dot{w}_b(x,y,\omega) = Y_{bp}(x,y,\omega)f_p(\omega) + Y_{bc}(x,y,\omega)f_c(\omega), \tag{4.1}$$

$$\dot{w}_c(\omega) = Y_{cp}(\omega)f_p(\omega) + Y_{cc}(\omega)f_c(\omega), \tag{4.2}$$

where $f_p(\omega)$ is the phasor of the incident primary excitation and $f_c(\omega)$ is the phasor of the control excitation. The four mobility terms in Eq. (4.1) and (4.2) can be written by the following formulae [10]:

$$Y_{bp}(x,y,\omega)=\boldsymbol{\phi}(x,y)\mathbf{a}_p(\omega), \tag{4.3}$$

$$Y_{bc}(x,y,\omega)=\boldsymbol{\phi}(x,y)\mathbf{a}_c(\omega), \tag{4.4}$$

$$Y_{cp}(\omega)=\boldsymbol{\phi}_c(x_c,y_c)\mathbf{a}_p(\omega), \tag{4.5}$$

$$Y_{cc}(\omega)=\boldsymbol{\phi}_c(x_c,y_c)\mathbf{a}_c(\omega), \tag{4.6}$$

where $\boldsymbol{\phi}(x,y)$ and $\boldsymbol{\phi}_c(x_c,y_c)$ are row vectors with the first N natural modes of the plate calculated in a generic point (x,y) and in the control point (x_c,y_c) respectively:

$$\boldsymbol{\phi}(x,y)=\lfloor \phi_1(x,y) \quad \phi_2(x,y) \quad \ldots \quad \phi_N(x,y) \rfloor, \tag{4.7}$$

$$\boldsymbol{\phi}_c(x,y)=\lfloor \phi_1(x_c,y_c) \quad \phi_2(x_c,y_c) \quad \ldots \quad \phi_N(x_c,y_c) \rfloor, \tag{4.8}$$

and $\mathbf{a}_p(\omega)$, $\mathbf{a}_c(\omega)$ are column vectors with the first N modal responses of the plate due to either the primary or control excitation:

$$\mathbf{a}_p(\omega)=\begin{bmatrix} a_{p,1}(\omega) \\ a_{p,2}(\omega) \\ \vdots \\ a_{p,N}(\omega) \end{bmatrix}, \tag{4.9}$$

$$\mathbf{a}_c(\omega)=\begin{bmatrix} a_{c,1}(\omega) \\ a_{c,2}(\omega) \\ \vdots \\ a_{c,N}(\omega) \end{bmatrix}. \tag{4.10}$$

The terms in the primary modal response vector, $\mathbf{a}_p(\omega)$, are given by:

$$\mathbf{a}_p = j\omega \frac{\phi_{m,n}(x_p,y_p)}{\Lambda\left[\left(\omega_{m,n}^2(1+j\eta_s)-\omega^2\right]\right.}, \tag{4.11}$$

while the terms for the force in the control modal response vector, $\mathbf{a}_c(\omega)$, are given by:

$$\mathbf{a}_c = j\omega \frac{\phi_{m,n}(x_c, y_c)}{\Lambda\left[\left(\omega_{m,n}^2(1+j\eta_s)-\omega^2\right]\right.}, \tag{4.12}$$

where $\omega_{m,n}$ is the natural frequency of the (m,n)th natural mode of the plate, $\phi_{m,n}(x,y)$ is the (m,n)th natural mode of the plate at position (x,y), $\Lambda=\rho h l_x l_y/4$ is the modal normalization, ρ is the density of the plate, l and h are respectively the dimensions and thickness of the plate, and η_s the loss factor. The natural frequencies and modes of the plate at the position (x,y) are respectively:

$$\omega_{m,n}(x,y) = \sqrt{\frac{E_s h_s^2}{12\rho_s(1-\nu_s^2)}} \cdot \left[\left(\frac{m\pi}{l_x}\right)^2 + \left(\frac{n\pi}{l_y}\right)^2\right], \tag{4.13}$$

$$\phi_{m,n}(x,y) = \sin\left(\frac{m\pi x}{l_x}\right)\sin\left(\frac{n\pi y}{l_y}\right), \tag{4.14}$$

where E_s is the Young's modulus, and ν_s Poisson ratio of the material of the plate. From the previous definitions, the mobility functions of the Y_{cp} and Y_{cc} are given by the following expressions:

$$Y_{cp} = j\omega \sum_{m=1}^{\infty}\sum_{n=1}^{\infty} \frac{\phi_{m,n}(x_c, y_c)\phi_{m,n}(x_p, y_p)}{\Lambda\left[\left(\omega_{m,n}^2(1+j\eta_s)-\omega^2\right]\right.}, \tag{4.15}$$

$$Y_{cc} = j\omega \sum_{m=1}^{\infty}\sum_{n=1}^{\infty} \frac{\phi_{m,n}(x_c, y_c)\phi_{m,n}(x_c, y_c)}{\Lambda\left[\left(\omega_{m,n}^2(1+j\eta_s)-\omega^2\right]\right.}. \tag{4.16}$$

Table 5: *Geometry and physical parameters for the panel.*

Parameter	Value
Dimensions	l_x l_y=0.414x0.314 m
Thickness	h=1 mm
Mass density	ρ=2700 kg/m^3
Young's modulus	E_s=7.1x10^{10} N/m
Poisson ratio	ν_s=0.33
Loss factor	η_s=0.02
Position of the control system	x_c, y_c=0.33l_x, 0.71l_y
Position of the primary excitation	x_p, y_p=0.15l_x, 0.44l_y

4.2 Feedback Control with a velocity sensor–inertial actuator pair.

As shown in Figure 37, the response of a plate with an inertial actuator and an ideal velocity sensor at its base for the implementation of a feedback control loop is now considered.

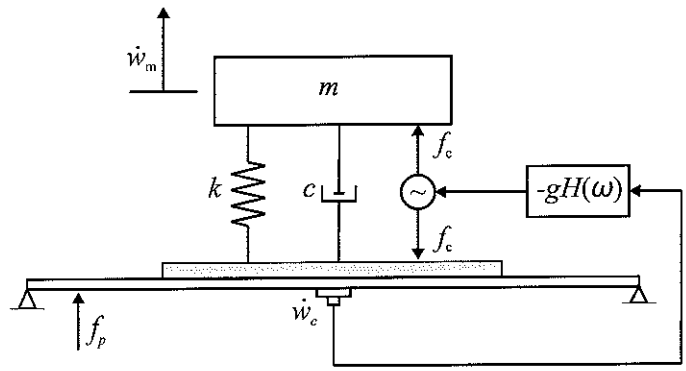

Figure 37: *Schema of an actuator mounted in a simple supported plate with an ideal collocated velocity sensor.*

Figure 38 shows in details the forces and displacements acting on the elements of the actuator which is mounted on the plate at the control point.

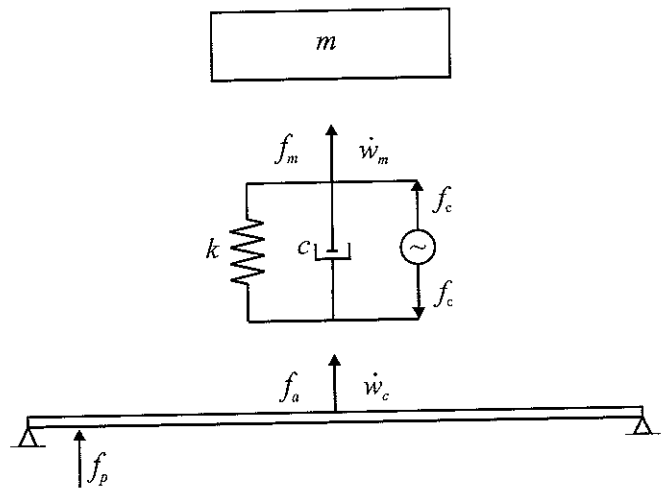

Figure 38: *Schema with the notation for the forces an displacement at the connecting points between the elements of the accelerometer which is mounted on an aluminium plate with a collocated force actuator.*

Table 6 : *Physical parameters for the inertial actuator.*

Parameter	Value
Mass	$m = 0.03$ Kg
Stiffness	$k = 118.45$ N/m
Critical damping	$c_c = 3.76$ N/ms^{-1}
Damping	$c = 0.75$
Natural frequency	$f_n = 10$ Hz
Transducer coefficient	$\Psi = 2.6$ N/A

In this case the velocity at a generic point of the plate $\dot{w}_b$ or at the control sensor position $\dot{w}_c$ and the velocity of the actuator mass $\dot{w}_m$ can be expressed using the following mobility formulae:

$$\dot{w}_b = Y_{bp} f_p + Y_{ba} f_a , \tag{4.17}$$

$$\begin{cases} \dot{w}_c = Y_{cp} f_p + Y_{cc} f_a \\ \dot{w}_m = Y_m f_m \end{cases}, \tag{4.18}$$

where Y_{cc} and Y_{ba} are the point motilities respectively at the control position (x_c, y_c) and a generic plate position (x, y) with reference to the force at the base of the actuator, Y_m

is the mobility function of the inertial mass which can be derived from Newton's second law:

$$f_m = m\ddot{w}_m \ , \tag{4.19}$$

so that:

$$Y_m = \frac{j\omega w_m}{f_m} = \frac{1}{j\omega m} \ . \tag{4.20}$$

The two equations in (4.18) can be written in the matrix form as follow:

$$\dot{\mathbf{w}} = \mathbf{Y}\mathbf{f} + \mathbf{Y}_p f_p \, , \tag{4.21}$$

where

$$\dot{\mathbf{w}} = \begin{Bmatrix} \dot{w}_c \\ \dot{w}_m \end{Bmatrix}, \tag{4.22}$$

$$\mathbf{Y} = \begin{pmatrix} Y_{cc} & 0 \\ 0 & Y_m \end{pmatrix}, \tag{4.23}$$

$$\mathbf{f} = \begin{Bmatrix} f_a \\ f_m \end{Bmatrix}, \tag{4.24}$$

$$\mathbf{Y}_p = \begin{Bmatrix} Y_{cp}^A \\ 0 \end{Bmatrix}. \tag{4.25}$$

The constitutive equation for the spring and damping elements in parallel could be written as follow:

$$f_a = -k(w_c - w_m) - c(\dot{w}_c - \dot{w}_m) = -k\left(\frac{\dot{w}_c}{j\omega} - \frac{\dot{w}_m}{j\omega}\right) - c\ (\dot{w}_c - \dot{w}_m), \tag{4.26}$$

$$f_m = -k(w_m - w_c) - c_1(\dot{w}_m - \dot{w}_c) = -k\left(\frac{\dot{w}_m}{j\omega} - \frac{\dot{w}_c}{j\omega}\right) - c\ (\dot{w}_m - \dot{w}_c). \tag{4.27}$$

where the relation $w(\omega) = \dot{w}(\omega)/j\omega$ was used. The two equations (4.26) and (4.27) can be written in matrix form as follows:

$$\mathbf{f} = -\mathbf{Z}\dot{\mathbf{w}}, \tag{4.28}$$

where

$$\mathbf{Z} = \begin{pmatrix} Z_{11} & Z_{12} \\ Z_{21} & Z_{22} \end{pmatrix}, \tag{4.29}$$

and

$$Z_{11} = Z_{22} = \left(\frac{k}{j\omega} + c \right), \tag{4.30}$$

$$Z_{12} = Z_{21} = -\left(\frac{k}{j\omega} + c \right). \tag{4.31}$$

In order to take into account the effect of the control force generated by the control actuator, equation (4.28) is rewritten as:

$$\mathbf{f} = -\mathbf{Z}\dot{\mathbf{w}} + \mathbf{h}_s f_c, \tag{4.32}$$

where

$$\mathbf{h}_s = \begin{Bmatrix} +1 \\ -1 \end{Bmatrix}, \tag{4.33}$$

and f_c is the control signal. Substituting equation (4.32) into equation (4.21) and solving with respect to the velocity vector, the following expression for the velocity of the control sensor and actuator mass are derived:

$$\dot{\mathbf{w}} = \mathbf{y}_p f_p + \mathbf{y}_c f_c, \tag{4.34}$$

where $\mathbf{y}_p$ and $\mathbf{y}_c$ are given by:

$$\mathbf{y}_p = (\mathbf{I} + \mathbf{YZ})^{-1}\mathbf{Y}_p, \tag{4.35}$$

$$\mathbf{y}_c = (\mathbf{I} + \mathbf{YZ})^{-1}\mathbf{Y}\mathbf{h}_s. \tag{4.36}$$

From Eq. (4.34) the velocity at the control sensor position $\dot{w}_c$ can be expressed as:

$$\dot{w}_c = Y_{cp}^A f_p + Y_{cc}^A f_c, \tag{4.37}$$

where

$$Y_{cp}^A = \mathbf{q}\mathbf{y}_p, \tag{4.38}$$

$$Y_{cc}^A = \mathbf{q}\mathbf{y}_c, \tag{4.39}$$

where $\mathbf{q}$ is a row vector given by:

$$\mathbf{q} = \lfloor 1 \quad 0 \rfloor. \tag{4.40}$$

Substitution of Eq. (4.34) into the Eq. (4.32) gives:

$$\mathbf{f} = \mathbf{z}_s f_c - \mathbf{Z}\mathbf{y}_p f_p, \tag{4.41}$$

where

$$\mathbf{z}_s = -\mathbf{Z}\mathbf{y}_c + \mathbf{h}_s. \tag{4.42}$$

The force f_a transmitted to the plate can therefore be obtained from Eq. (4.41):

$$f_a = \mathbf{q}\mathbf{z}_s f_c - \mathbf{q}\mathbf{Z}\mathbf{y}_p f_p, \tag{4.43}$$

where $\mathbf{q}$ is given in Eq. (4.40). Equation (4.43) gives the force transmitted from the inertial actuator to the plate structure when a primary force f_p is also acting on the plate. In the case with no primary force, i.e. $f_p = 0$, then, as shown in Figure 39, the force f_a transmitted to the base per unit of control force f_c can be derived. Below the fundamental resonance of the actuator there is hardly any transmitted force to the structure. At resonance the transmitted force f_a is much greater than the control force f_c and above resonance the transmitted force has constant amplitude equal to the control force. There are little drops of the transmitted force f_a in correspondence to the plate resonances since little reaction is provided by the plate at these frequencies. Also, at frequencies below the resonance frequency of the actuator, the transmitted force is out of phase with the control force while, above the actuator resonance it is in phase with the actuator force.

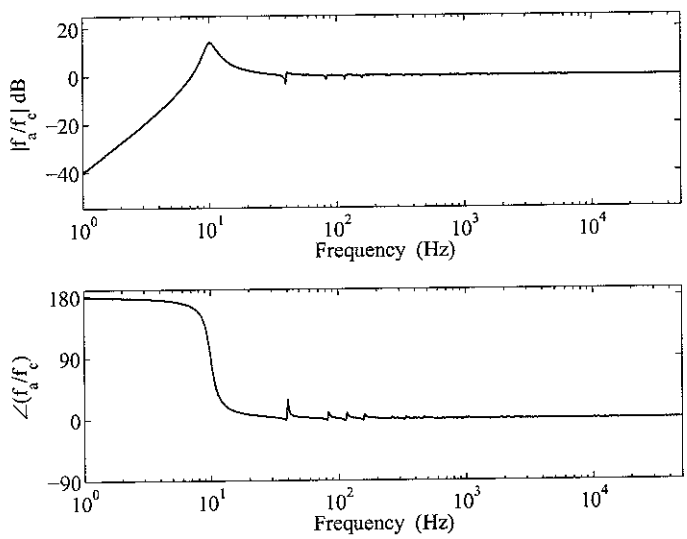

Figure 39: *Force transmitted to the base structure per unit of control force.*

The transverse velocity in a generic point of the plate $\dot{w}_b$ can be calculated substituting Eq. (4.43) into Eq. (4.17), so that:

$$\dot{w}_b = Y_{bp}^A f_p + Y_{bc}^A f_c, \tag{4.44}$$

where Y_{bp}^A and Y_{bc}^A for this case are given by:

$$Y_{bp}^A = Y_{bp} - Y_{ba}\mathbf{qZy}_p, \tag{4.45}$$

$$Y_{bc}^A = Y_{ba}\mathbf{qz}_s. \tag{4.46}$$

4.3 Feedback control with a velocity sensor–inertial electro–dynamic actuator driven current.

The system studied in this section consists in an inertial electro–dynamic actuator mounted on a simply supported plate with an ideal velocity sensor at its base for the implementation of a feedback active vibration control system with current control.

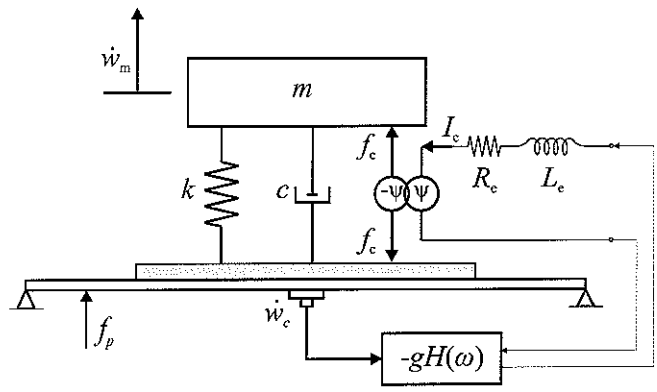

Figure 40: *Schema of an inertial electro–dynamic actuator with current control mounted on a simply supported plate.*

As shown in Figure 40, the coil–magnet electrodynamic actuator is modelled in terms of a resistance R_e and inductance L_e for the coil. According to Biot–Savart's law, the reactive force generated by the coil–magnet system is directly proportional to the current I_c in the coil [4].

$$f_c = \psi I_c, \tag{4.47}$$

where ψ is the transducer coefficient given by Table 7. Substituting Eq. (4.47) into Equation (4.37) the velocity at the sensor point due to the primary force f_p and control current I_c can be obtained:

$$\dot{w}_c = Y_{cp}^A f_p + Y_{cc}^I I_c, \tag{4.48}$$

where Y_{cc}^I is the point mobility at the control position when a current control is used:

$$Y_{cc}^I = \psi Y_{cc}^A. \tag{4.49}$$

Substituting Eq. (4.47) into Eq. (4.43) the transmitted force f_a at the base using a current control can be obtained:

$$f_a = \mathbf{q}\mathbf{z}_s \psi\, I_c - \mathbf{q}\mathbf{Z}\mathbf{y}_p f_p . \tag{4.50}$$

Equation (4.50) gives the force transmitted from the inertial actuator to the plate when a primary force f_p is also acting on the plate. In the case with no primary force, i.e. $f_p = 0$, then, as shown in Figure 41 the force transmitted to the base per unit driving current is found to be similar to that shown in Figure 39 for the ideal inertial actuator but shifted by $10\log_{10}|1/\psi|$, which considering the properties listed in Table 7 corresponds to 4.1 dB.

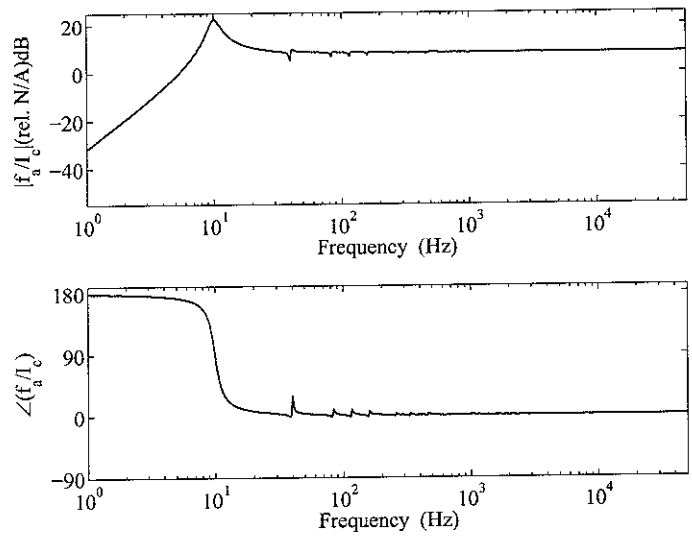

Figure 41: *Force transmitted to the base structure per unit driving current by the coil.*

The transverse velocity on a generic point $\dot{w}_b$ of the plate can be calculated substituting Eq. (4.50) into Eq. (4.17):

$$\dot{w}_b = Y^I_{bp} f_p + Y^I_{bc} I_c , \tag{4.51}$$

where Y^I_{bp} and Y^I_{bc} for this case are given by:

$$Y^I_{bp} = Y_{bp} - Y_{ba}\mathbf{q}\mathbf{Z}\mathbf{y}_p , \tag{4.52}$$

$$Y^I_{bc} = \psi Y_{ba}\mathbf{q}\mathbf{z}_s . \tag{4.53}$$

4.4 Feedback control with an inertial electro–dynamic actuator with voltage control.

The system studied in this section consists in the same inertial electro–dynamic actuator mounted on a simply supported plate with an ideal velocity sensor at its base for the implementation of a feedback control loop with voltage control as shown in Figure 42.

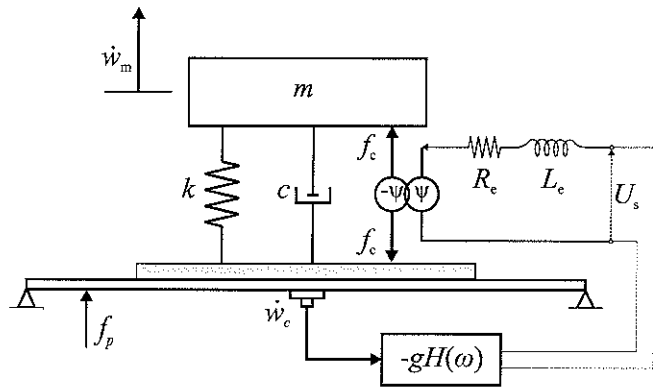

Figure 42: *Schema of an inertial electro–dynamic actuator with voltage control mounted on a simply supported plate.*

Table 7: *Physical parameters for the inertial electro–dynamic actuator.*

Parameter	Value
Transducer coefficient of the coil	$\Psi = 2.6$ N/A
Resistance of the coil	$R_e = 20\ \Omega$
Inductance of the coil	$L_e = 0.002$ H

In this case, because of the back e.m.f. effect generated by the relative motion between the mass and the coil, the current I_c in the coil of this inertial electro–dynamic actuator is governed by the following relation [4]:

$$R_e I_c + L_e \frac{dI_c}{dt} = U_s - \psi \mathbf{h}_t \dot{\mathbf{w}}\,, \tag{4.54}$$

where R_e is the resistance and L_e the inductance of the coil, U_s is the applied voltage and $-\psi\ \mathbf{h}_t\dot{\mathbf{w}}$ is the back electromotive force due to the vibration of the inertial mass with respect to the base of the actuator.

Considering harmonic vibration and electric functions, Eq. (4.54) becomes:

$$(R_e + j\omega L_e)I_c = U_s - \psi\ \mathbf{h}_t\dot{\mathbf{w}} \tag{4.55}$$

Thus substituting the current I_c from the Eq. (4.55) into Eq. (4.47) the electro–magnetic actuation force, f_c when a voltage control is used can be expressed as:

$$f_c = \psi\frac{U_s - \psi\ \mathbf{h}_t\dot{\mathbf{w}}}{Z_e}, \tag{4.56}$$

where

$$\mathbf{h}_t = \lfloor -1 \quad 1 \rfloor, \tag{4.57}$$

$$Z_e = R_e + j\omega L_e, \tag{4.58}$$

Substituting Eq. (4.56) into the Eq. (4.34) and solving with respect to the velocity vector, the following expression can be obtained:

$$\dot{\mathbf{w}} = \mathbf{Q}_{cp}f_p + \mathbf{Q}_{cc}U_s, \tag{4.59}$$

where

$$\mathbf{Q}_{cp} = \left(I + \mathbf{y}_c\frac{\psi^2\mathbf{h}_t}{Z_e}\right)^{-1}\mathbf{y}_p, \tag{4.60}$$

$$\mathbf{Q}_{cc} = \left(I + \mathbf{y}_c\frac{\psi^2\mathbf{h}_t}{Z_e}\right)^{-1}\mathbf{y}_c\frac{\psi}{Z_e}, \tag{4.61}$$

From Eq. (4.59) the velocity at the control sensor position can be expressed as:

$$\dot{w}_c = Y_{cp}^U f_p + Y_{cc}^U U_s, \tag{4.62}$$

where in this case

$$Y_{cp}^U = \mathbf{q}\mathbf{Q}_{cp}, \tag{4.63}$$

$$Y_{cc}^U = \mathbf{q}\mathbf{Q}_{cc}. \tag{4.64}$$

and

$$\mathbf{q} = \begin{bmatrix} 1 & 0 \end{bmatrix}. \tag{4.65}$$

Substituting the current in the coil I_c from Eq. (4.55) and velocity vector $\dot{\mathbf{w}}$ from Eq. (4.59) into Eq. (4.50), the actuator force f_a transmitted to the plate using a voltage control signal can be obtained:

$$f_a = \frac{\mathbf{q}\mathbf{z}_s\psi}{Z_e}\left(1-\psi\mathbf{h}_t\mathbf{Q}_{cc}\right)U_s - \left(\mathbf{q}\mathbf{Z}\mathbf{y}_p + \frac{\mathbf{q}\mathbf{z}_s\psi^2\mathbf{h}_t\mathbf{Q}_{cp}}{Z_e}\right)f_p, \tag{4.66}$$

Considering the case with no primary force, i.e. $f_p = 0$, the force transmitted to the base per unit of driving current is derived as shown in Figure 43.

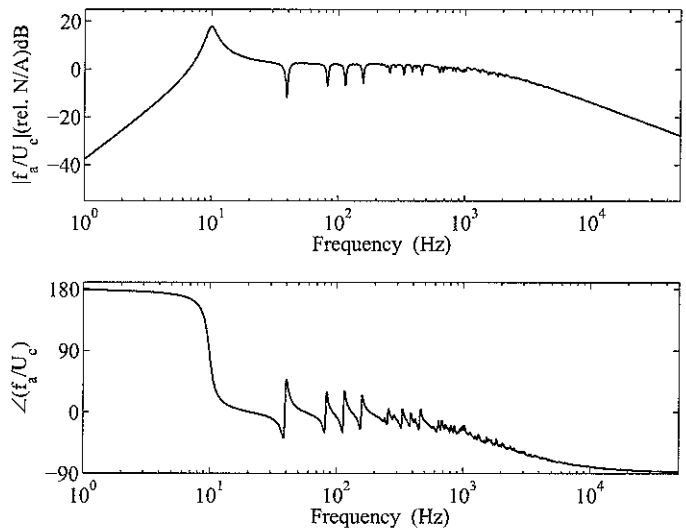

Figure 43: *Force transmitted to the base structure per unit driving voltage by the coil.*

Figure 43 shows similar plot to that found for the current driven actuator, except that at higher frequencies the transmitted force is characterised by amplitude roll off and a phase lag which are due to the electric inductance effect which is similar to a mass effect. Also, the voltage driven the actuator is characterised by larger drops of the transmitted force at the resonance frequencies of the plate structure. The transverse velocity in a generic point $\dot{w}_b$ can be calculated substituting Eq. (4.66) into Eq. (4.17):

$$\dot{w}_b = Y_{bp}^U f_p + Y_{bc}^U U_c\,, \tag{4.67}$$

Where Y_{bp}^U and Y_{bc}^U are given by the following expressions:

$$Y_{bp}^{U} = Y_{bp} - Y_{ba}\left(\mathbf{qZy}_{p} + \frac{\mathbf{qz}_{s}\mathbf{h}_{t}\mathbf{Q}_{cc}}{Z_{e}}\right), \tag{4.68}$$

$$Y_{bc}^{U} = Y_{ba}\frac{\mathbf{qz}_{s}\psi}{Z_{e}}\left(1+\psi\mathbf{h}_{t}\mathbf{Q}_{cc}\right). \tag{4.69}$$

4.5 Stability analysis.

The stability analysis for the four control systems with a) the ideal point force actuator, b) inertial force actuator, and inertial electro–dynamic actuator with c) current control and d) voltage control can be carried out with reference to the classic rejection feedback block diagram shown in Figure 44 using the appropriate mobility functions Y_{cp} and Y_{cc} (Y_{cp}, Y_{cc} or Y_{cp}^{A}, Y_{cc}^{A} or Y_{cp}^{A}, Y_{cc}^{I} or Y_{cp}^{U}, Y_{cc}^{U}) for the control arrangement under study.

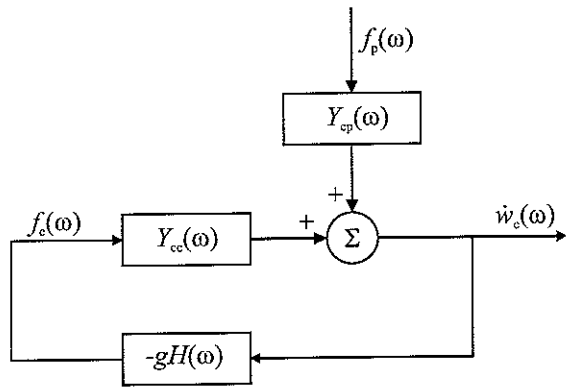

Figure 44: *Block diagrams of feedback control system implemented on the plate.*

Considering first the system with the ideal point force and inertial force actuators, the control force is given by:

$$f_{c}(\omega) = -gH(\omega)\dot{w}_{c}(\omega), \tag{4.70}$$

while for the current–driven and voltage–driven inertial electro–dynamic actuator the control current and control voltage are given respectively by:

$$I_{c} = -gH(\omega)\dot{w}_{c}, \tag{4.71}$$

and

$$U_c = -gH(\omega)\dot{w}_c, \tag{4.72}$$

where $H(\omega)$ is the control function. Substituting Eq. (4.70) into Eq. (4.2) and Eq. (4.37) and solving for $\dot{w}_c$, the velocity at control point for the point force actuator and for the inertial force actuator are derived with reference to the primary excitation by:

$$\dot{w}_c = \frac{Y_{cp}}{1 + gH(\omega)Y_{cc}} f_p, \tag{4.73}$$

$$\dot{w}_c = \frac{Y_{cp}^A}{1 + gH(\omega)Y_{cc}^A} f_p, \tag{4.74}$$

where $G_P = H(\omega)Y_{cc}$ and $G_A = H(\omega)Y_{cc}^A$ are the open loop frequency response functions between the control velocity and either the control point force or inertial actuator reactive control force.

For the case of the inertial electro–dynamic actuator, substituting Eq. (4.71) into Eq. (4.48) and Eq. (4.72) into Eq. (4.62) and solving for $\dot{w}_c$, the velocity at the control point for both cases, current and voltage control, are respectively given by:

$$\dot{w}_c = \frac{Y_{cp}^A}{1 + gH(\omega)Y_{cc}^I} f_p, \tag{4.75}$$

$$\dot{w}_c = \frac{Y_{cp}^I}{1 + gH(\omega)Y_{cc}^I} f_p, \tag{4.76}$$

where $G_I = H(\omega)Y_{cc}^I$ and $G_U = H(\omega)Y_{cc}^U$ are the open loop frequency response functions between the control velocity and either the current ($G_I = w_c^I / I_c$) or the voltage ($G_U = w_c^U / U_c$) driven to the coil.

As anticipated in the previous chapters if the real parts of G_P, G_A, G_I or G_U are positive real for all frequencies, then (4.73), (4.74), (4.75) and (4.76) show that $\dot{w}_c / f_p < 1$ for any control gain and frequency. Thus vibration control is obtained without the danger of instabilities. Considering the ideal point force actuator, the transverses velocities in a generic point of the plate when there is control can be calculated substituting Equations (4.73) and (4.70) into Eq. (4.1) which solving for $\dot{w}_b$ gives the closed loop response:

$$\dot{w}_b = \left(Y_{bp} - Y_{bc} \frac{gH(\omega)Y_{cp}}{1 + H(\omega)Y_{cc}} \right) f_p . \tag{4.77}$$

Considering the inertial actuator, then substituting Equations (4.70) and (4.74) into Eq. (4.44) and solving for $\dot{w}_b$ the closed loop response is given by:

$$\dot{w}_b = \left[Y_{bp} - Y_{bc} \left(\mathbf{qz}_s \frac{gH(\omega)Y_{cp}^A}{1 + H(\omega)Y_{cc}^A} + \mathbf{qZy}_p \right) \right] f_p . \tag{4.78}$$

Finally considering the inertial electro–dynamic actuator, substituting (4.75) and (4.71) into Eq. (4.51) or substituting Equations (4.76) and (4.72) into Eq. (4.67) and solving for $\dot{w}_b$ gives the closed loop response for the current and voltage driven control schemes respectively:

$$\dot{w}_b = \left[Y_{bp} - Y_{bc} \left(\mathbf{qz}_s \frac{gH(\omega)Y_{cp}^I}{1 + H(\omega)Y_{cc}^I} + \mathbf{qZy}_p \right) \right] f_p , \tag{4.79}$$

$$\dot{w}_b = \left\{ Y_{bp} - Y_{bc} \left[\frac{\mathbf{qz}_s \psi}{Z_e} \left(\left(1 - \psi\, \mathbf{h}_t \mathbf{Q}_{cc}\right) \frac{gH(\omega)Y_{cp}^U}{1 + H(\omega)Y_{cc}^U} + \psi\, \mathbf{h}_t \mathbf{Q}_{cp} \right) + \mathbf{qZy}_p \right] \right\} f_p . \tag{4.80}$$

In the following points the bode and Nyquist plots for the four control systems will be studied in order to asses their stability properties.

§ Proportional Control.

The control function in this case is $H(\omega)=-g$:

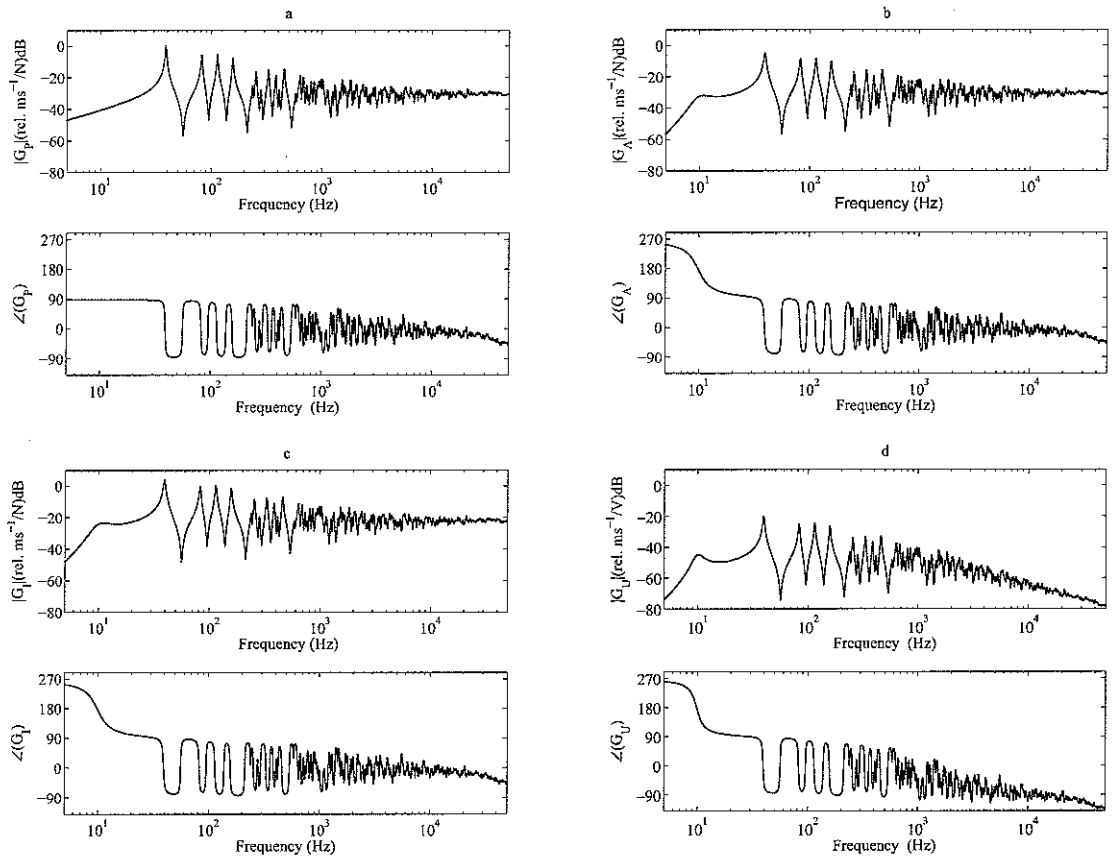

Figure 45: *Bode plots of the open loop FRF of the feedback systems using: a) a point force, b) inertial force actuator, inertial electro–dynamic actuator with c) current and d) voltage control in the 1-50 KHz frequency range when a Proportional control function is used.*

The phase plot in Figure 45a confirms that the open loop frequency response function HY_{cc} of the control system with an ideal control force is positive real and thus provides an unconditionally stable control system. Alternatively the phase plots of the control systems with the inertial force actuator or inertial electro–dynamic actuator with current or voltage control (Figure 45b, c and d) indicate that the phase plot starts from +270°, drops to +90° after the resonance of the actuator and then oscillates between +90° and –90° for the resonances of the plate. The first 180° phase drop from 270° to 90° is due to the inertial actuator which, as shown in Figure 39, Figure 41 and Figure 43, below the actuator resonance frequency transmits a control force to the plate 180° out of phase with the control force signal. In the voltage control case (Figure 45c) at higher frequencies above 1 KHz, the phase plot goes to values beyond –90° because of the coil inductance effect at higher frequencies. This inductance effect also brings

down the amplitude of the open loop response function at higher frequencies. The plant responses for the three systems with inertial actuators are similar to that of the two DOF system studied in chapter 3 except that in these cases the base system is a distributed structure with ∞ degrees of freedom which introduces many resonances as clearly highlighted by the peaks in the open loop response function.

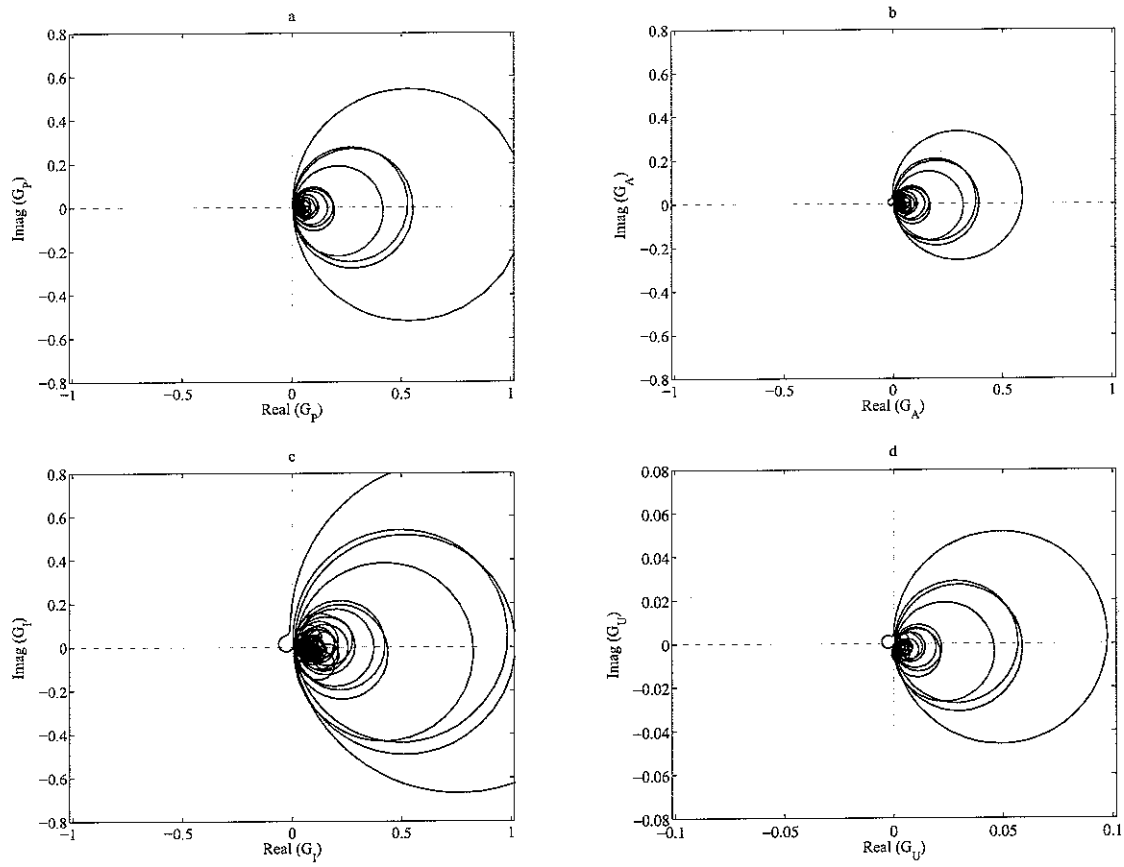

Figure 46: *Nyquist plots of the open loop FRF of the feedback systems using: a) a point force, b) inertial force actuator, inertial electro–dynamic actuator with c) current and d) voltage control in the 1-50 KHz frequency range when a Proportional control function is used.*

The Nyquist plot of Figure 46a shows that the polar plot of the open loop response function of the system with an ideal control force is entirely confined on the right hand side quadrants, which also confirms the unconditional stability of Proportional Control. However the Nyquist plot of the control systems with the inertial force actuator and inertial electro–dynamic actuator with current and voltage control (Figure 46b, c and d) show one circle on the left hand side quadrants which is due to the resonance of the actuator while the right hand side circles are due to the resonances of the plate. The actuator circle is confined on the left hand side quadrants which suggest that the system is only conditionally stable since for large control gains it can encircle the Nyquist

instability point. The higher frequencies effect of the voltage–driven inertial electro–dynamic actuator is better seen in the zoom Nyquist plot in the Figure 47d. This plot shows that the open loop sensor actuator response function of the voltage–driven inertial actuator system is characterised by high frequencies circles that goes to the negative real part.

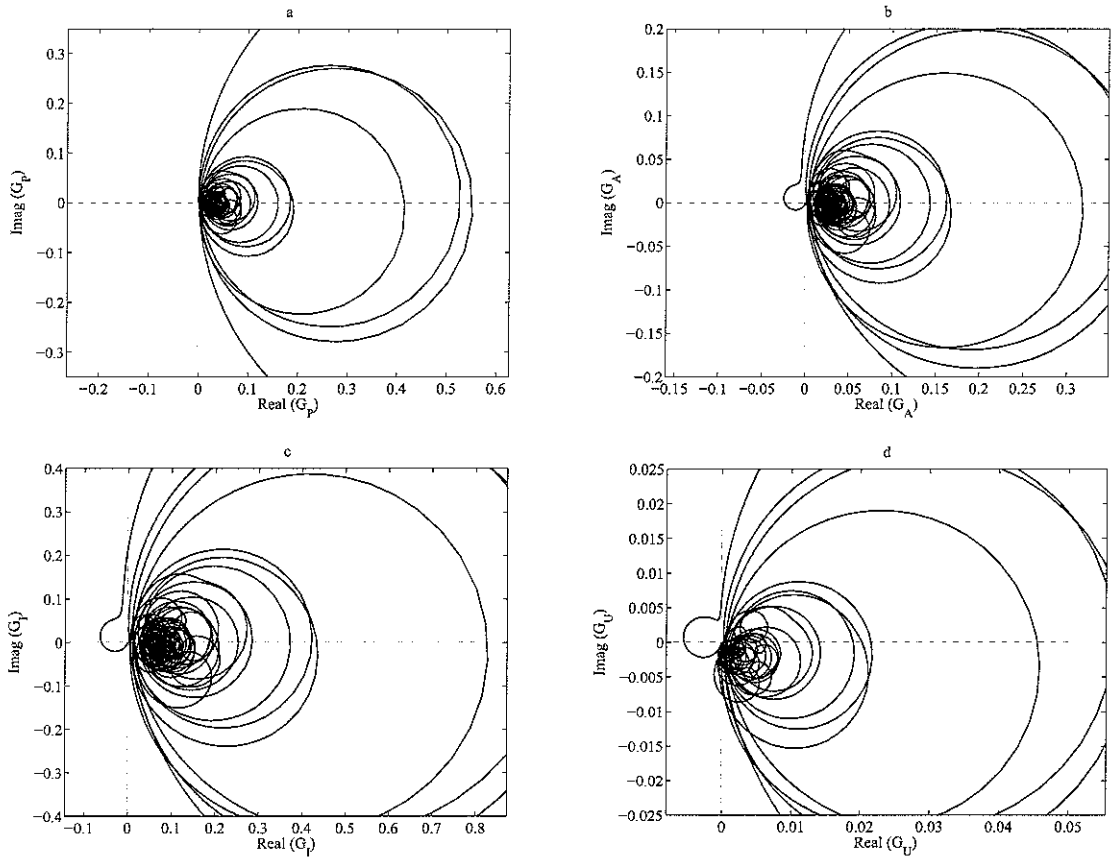

Figure 47: *Zoom of the Nyquist plots show in Figure 46.*

In general, the zoom plots in Figure 47 highlights that apart from the ideal case with a point force actuator, the low frequency resonance introduced by the mass–spring inertial actuator occupies the circle of unit radius and centre in the Nyquist critical point so that, even for moderate control gains that ensures conditional stability, control spillover effects occurs around the actuator resonance frequency.

Therefore having a "small" actuator resonance frequency is very important in order to get a stable control loop with large control gains but also to get little control spillover effects at low frequency around the resonance of the actuator. This "low amplitude" resonance of the actuator is normally obtained by designing an actuator with low natural frequency. There is however an intrinsic limit to achieve this since the stiffness of

the actuator must be large enough to suspend the mass without a too big static deflection, therefore a compromise must be found between a stiff enough spring to support the static weigh of the suspended mass an a soft enough spring to guarantee a low fundamental resonance frequency of the actuator. Further improvements can be made by adding and internal velocity feedback loop to the actuator in order to create active damping on the actuator that reduces the amplitude of its resonance [12].

Also an integral displacement feedback loop can be added so that a self levelling system can be obtained which would enable the use of very soft suspension systems for the inertial mass [13].

§ Integral Control.

In this case the control function is $H(\omega) = -g / j\omega$:

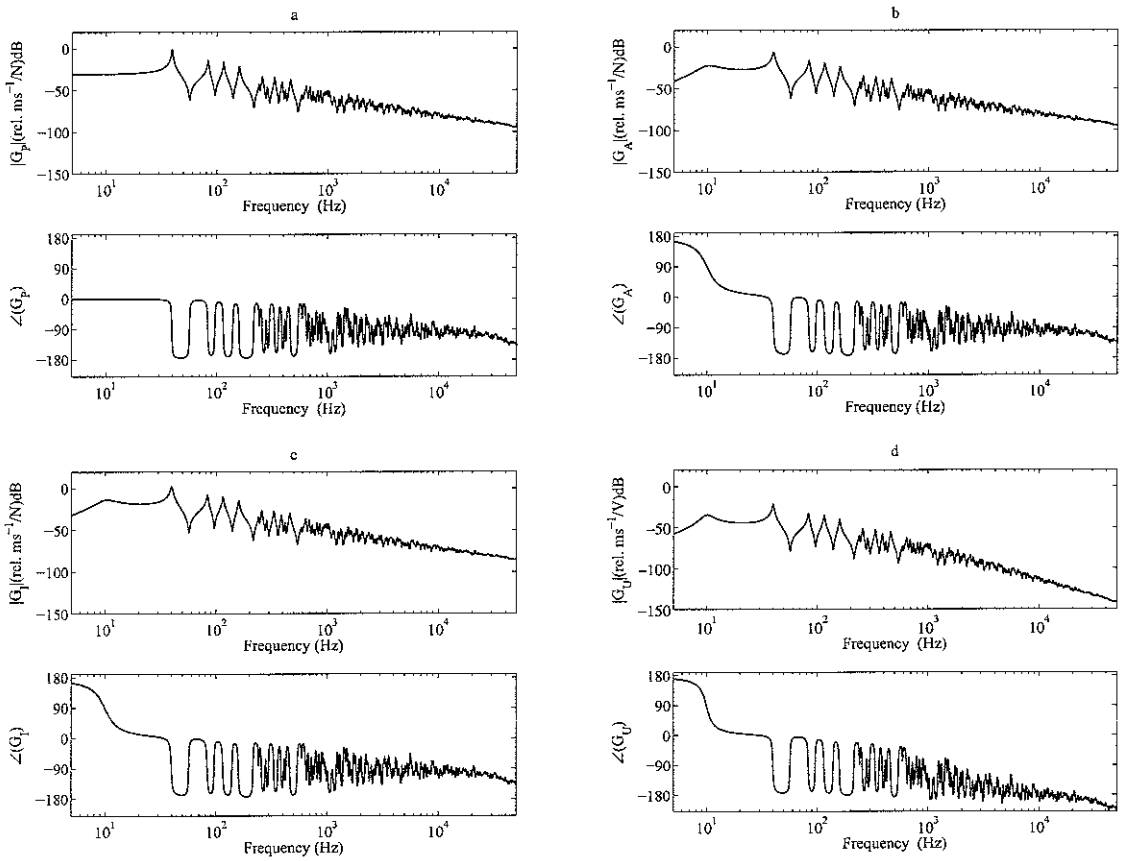

Figure 48: *Bode plots of the open loop FRF of the feedback systems using: a) a point force, b) inertial force actuator, inertial electro–dynamic actuator with c) current and d) voltage control in the 1-50 KHz frequency range when an Integral control function is used.*

As shown in Figure 48a, the phase plot indicates that the phase of the open loop sensor–actuator frequency response function HY_{cc} of the control system with an ideal control force exceed –90° and the amplitude goes down at higher frequencies. Alternatively the phase plots of the control systems with the inertial force actuator and inertial electro–dynamic actuator (Figure 48b, c and d) indicate that the phase of the open loop sensor–actuator frequency response function starts from 180°, drops to 0° at the resonance of the inertial actuator and then oscillates between 0 and 180° at higher frequencies above the first resonance of the plate. As discussed above, this is due to the actuator dynamics which as shown in Figures 39, 41 and 43 gives a transmitted force 180° out of phase at frequencies below its resonances. In this control case the amplitude of the open loop tends to decrease with frequency because of the integration 1/jω effect. For the voltage–driven inertial actuator this effect is even higher because of the inductance effect which also introduces an extra phase lag and amplitude drop at higher frequencies, as shown in Figure 48d.

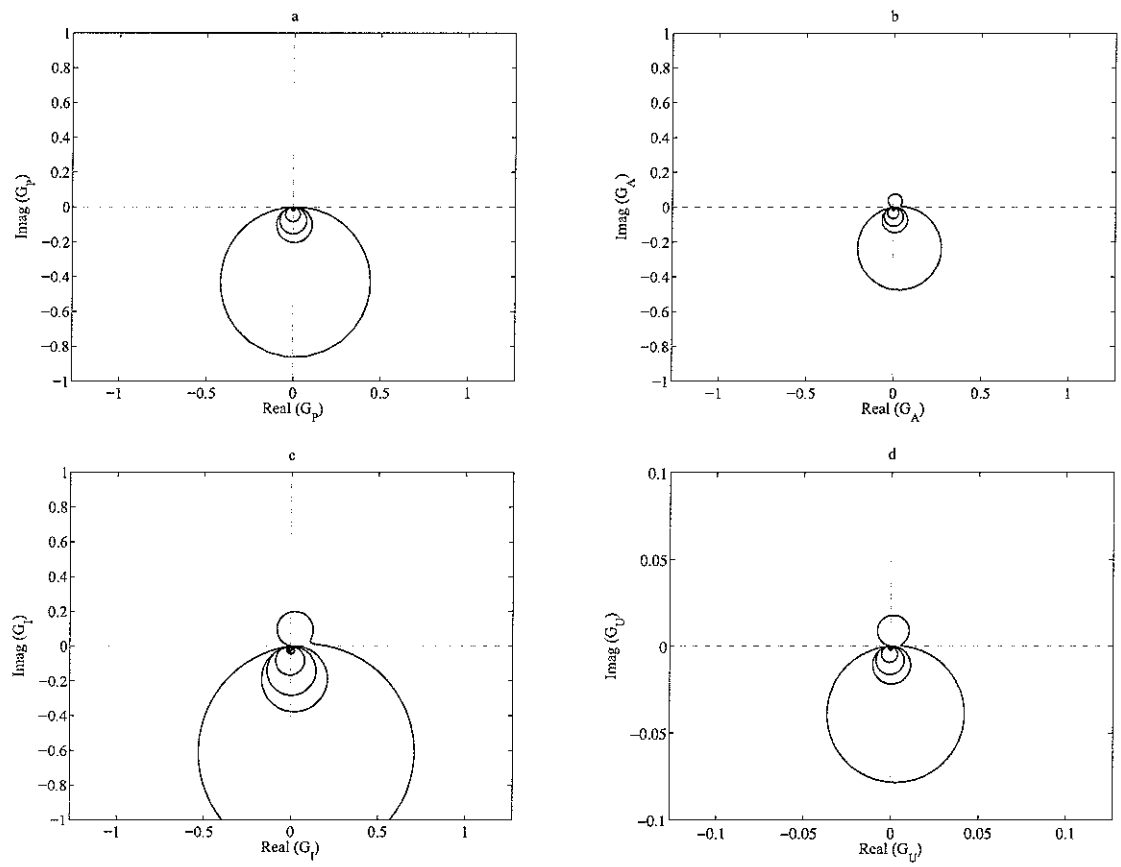

Figure 49: *Nyquist plots of the open loop FRF of the feedback systems using: a) a point force, b) inertial force actuator, inertial electro–dynamic actuator with c) current and d) voltage control in the 1-50 KHz frequency range when an Integral control function is used.*

The Nyquist plot of HY_{cc} for the control system with ideal control force in Figure 49a is characterised by circles which occupy the bottom quadrants only. This is due to the –90° phase lag which is added by the Integral Control. The system is therefore bound to be stable although spillover effects may occur at higher frequencies which could turn up to instabilities in case the system is perturbed by external disturbances. The Nyquist plot of HY_{cc} the control system with the inertial actuator (Figure 49b, c and d) show one circle on the top side quadrants, which is due to the actuator–resonance and others on the bottom side quadrants, which are due to the resonance of the plate. The zoom plots in Figure 50 show that the locus of HY_{cc} never crosses the real negative axis except for the inertial electro–dynamic actuator with voltage control system which has higher frequencies circles crossing the real negative axis because of the phase lag introduced by the inductance. In general, when integral control is implemented the system can go unstable, both at low and high frequencies, if external perturbations were to modify the system.

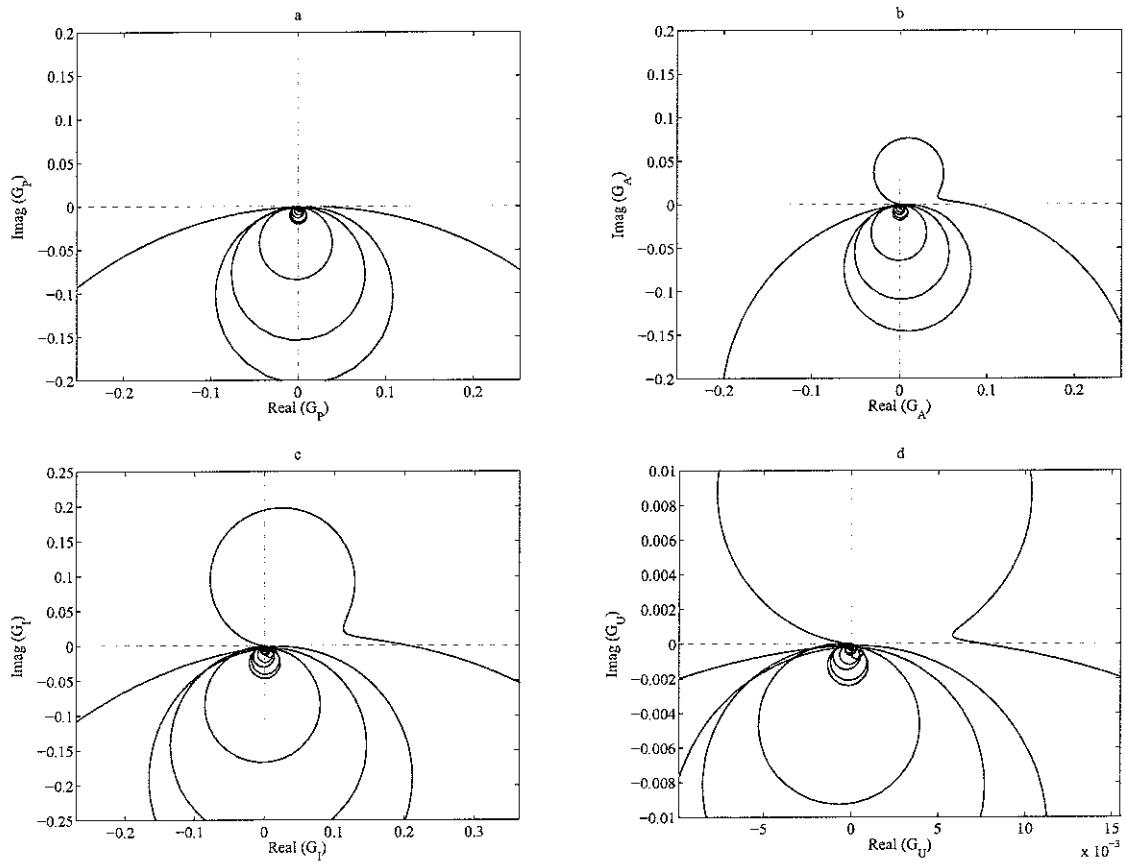

Figure 50: *Zoom of the Nyquist plots show in Figure 49.*

§ Derivative Control.

In this case the control function is $H(\omega) = -j\omega g$:

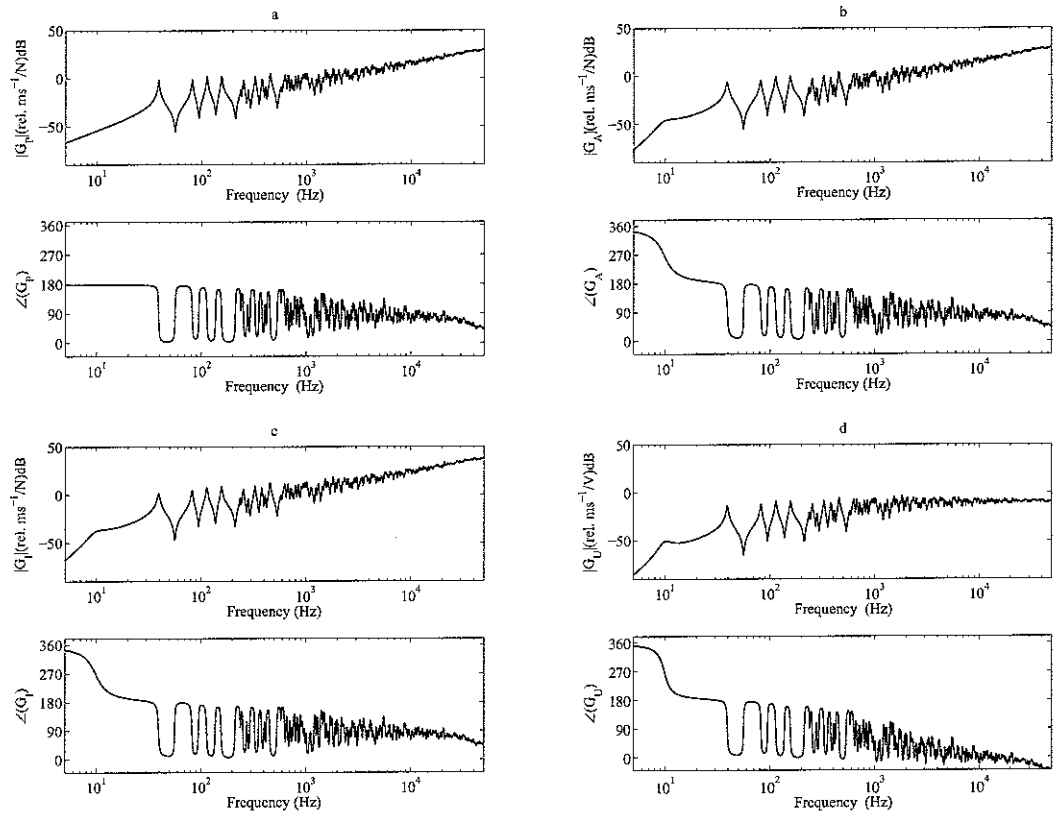

Figure 51: *Bode plots of the open loop FRF of the feedback systems using: a) a point force, b) inertial force actuator, inertial electro–dynamic actuator with c) current and d) voltage control in the 1-50 KHz frequency range when a Derivative control function is used.*

As shown in Figure 51a, the phase plot indicates that the phase of the open loop sensor–point frequency response function HY_{cc} for the control system with the ideal force actuator oscillates between 180° and 0° and the amplitude goes up with frequency. This is due to the +90° phase lead effect generated by the derivative controller. Alternatively in the case of the control system with the inertial actuator (Figure 51b, c and d) the phase plot starts from +360°, drops to 180° after the resonance of the actuator and then oscillates between 180° and 0° and goes beyond 0° for the voltage–driven actuator. Also in this case the 180° phase shift at the actuator resonance frequency is due to the dynamics of the actuator which, at frequencies below this resonance generates a transmitted force with phase opposite to that of the control input. As shown in the amplitude plots in the four pictures, the derivative control magnifies the amplitude proportionally to frequency. However, this effect is mitigated by the inductance effect of the driving–coil in the case of voltage–driven actuator.

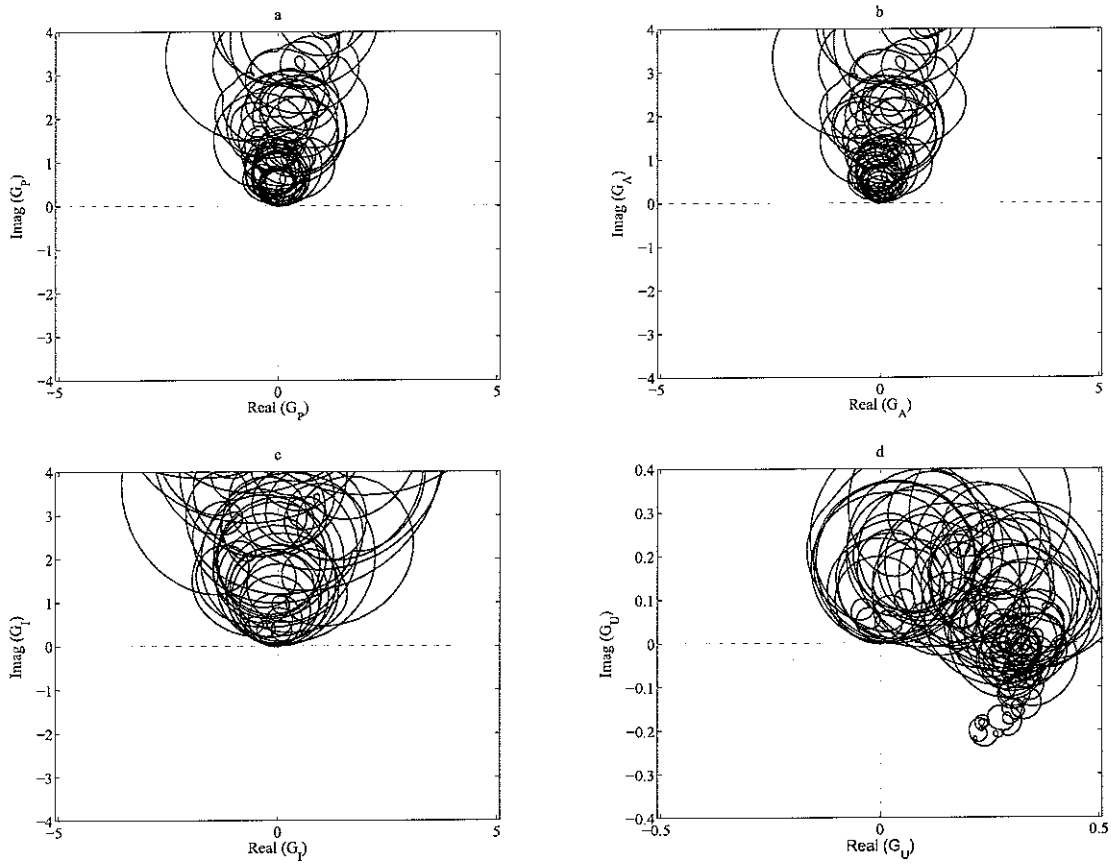

Figure 52: *Nyquist plots of the open loop FRF of the feedback systems using: a) a point force, b) inertial force actuator, inertial electro–dynamic actuator with c) current and d) voltage control in the 1-50 KHz frequency range when a Derivative control function is used.*

The Nyquist plot of HY_{cc}, with the ideal point force actuator in Figure 52a shows that the frequency response function is not confined on the right hand side quadrants. In fact the Nyquist plot is characterised by circles which occupy the two top quadrants. Thus, in principle, the control system is unconditionally stable although same of the low frequencies circles are very close to the Nyquist instability point as it is shown in more details in Figure 53a. Thus, the system is conditionally stable and prone to control spillover effects at low frequencies where the locus of HY_{cc} enters the circle of unit radius and centre (-1, j0). In the cases of the control systems with either the inertial force or inertial electro–dynamic actuators, Figure 52b, c, d and Figure 53b, c, d show one circle on the bottom quadrants which is due to the resonance of the actuator and others circles for the resonances of the plate on the top quadrants. Figure 53b, c and d show that in these cases the locus crosses the negative real axis and thus the systems are only conditionally stable. Moreover, even for moderate control gains they are likely to generate high control spillover effects.

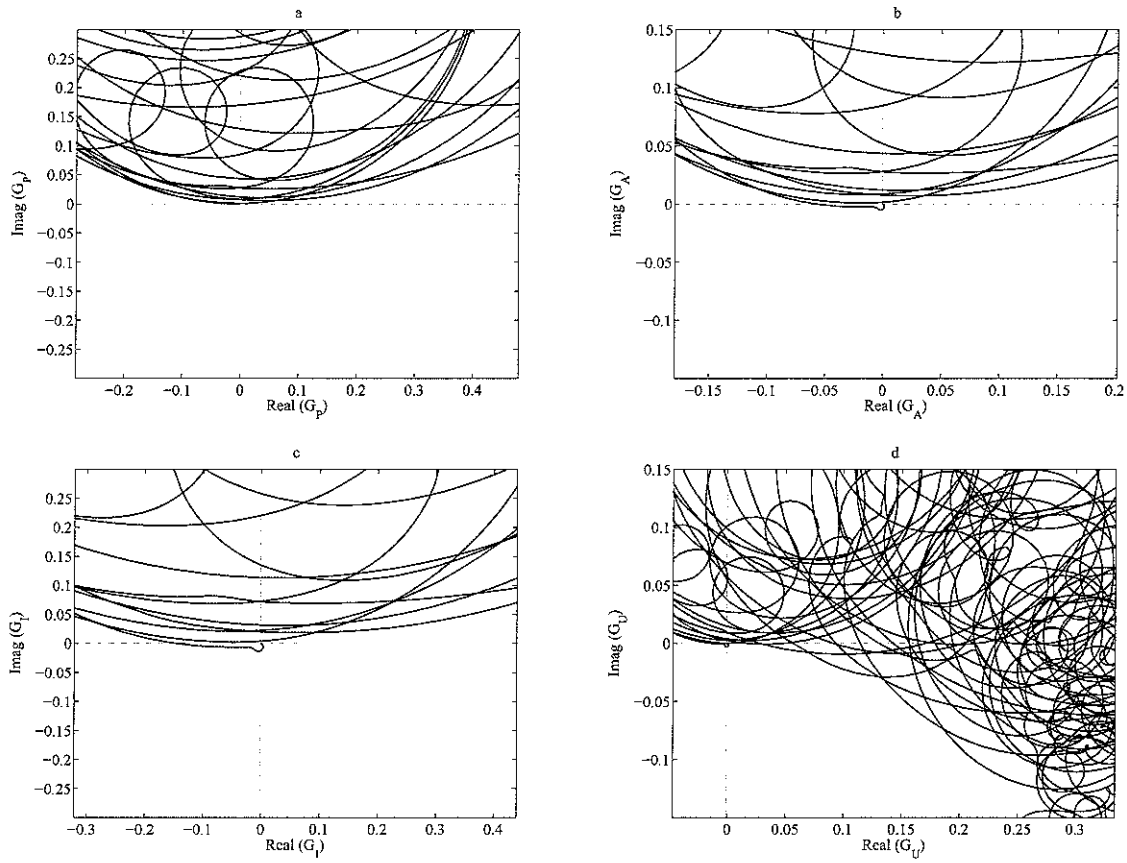

Figure 53: *Zoom of the Nyquist plots show in Figure 52.*

§ Proportional–Integral–Derivative (PID) Control.

The control function in this case is a combination of Proportional–Integral–Derivative control functions; $H(\omega)=-g\{\ k_P+k_I/j\omega+j\omega\ k_D\ \}$, where k_P, k_I and k_D are Proportional, Integral and Derivative Control constants respectively. These constants have been selected in such a way as to keep the first resonance of the panel constant when the control gain is raised. Since the first resonance of the panel corresponds to that of the base system considered in Chapter 3 for the two degrees of freedom model, then the constants are the same as those in Table 4 and the control function that is shown in Figure 21.

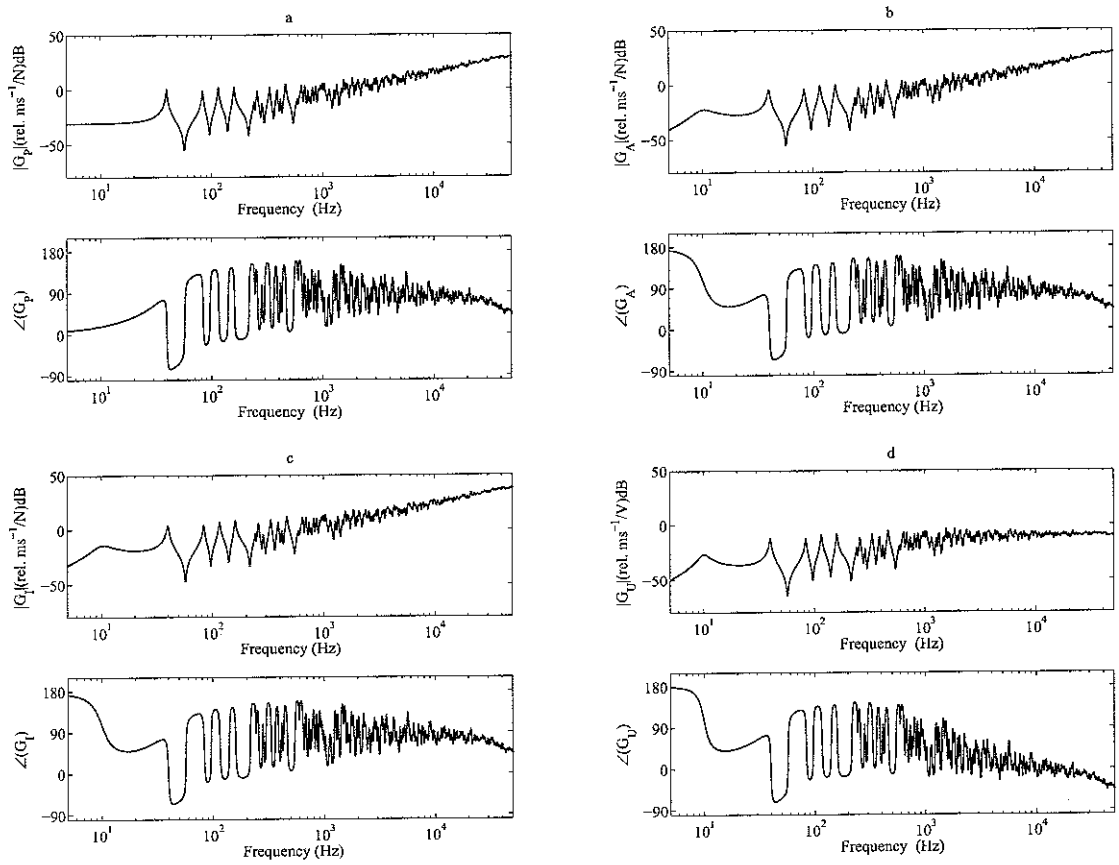

Figure 54: *Bode plots of the open loop FRF of the feedback systems using: a) a point force, b) inertial force actuator, inertial electro–dynamic actuator with c) current and d) voltage control in the 1-50 KHz frequency range when a PID control function is used.*

As shown in Figure 54a, in this case the open loop sensor–actuator HY_{cc} frequency response function for the control system with an ideal force actuator exceed +90° between the first resonance of the plate and 10 KHz. This is due to the effect of Derivative control above the first resonance of the plate. Alternatively in the case of the control system with either the inertial force or electro–dynamic actuator (Figure 54b, c and

d) the phase plot starts from +180°, drops to 0°, oscillates between –45° and +45° once and then oscillates between 0° and 180° above the first resonance of the plate. Also the higher frequency derivative effect in the controller produce a constant rise of amplitude with frequency of the open loop response function when the voltage–driven inertial actuator is used, this higher frequency effect of the derivative control is mitigated by the inductance effect of the coil however at the expenses of an additional phase lag.

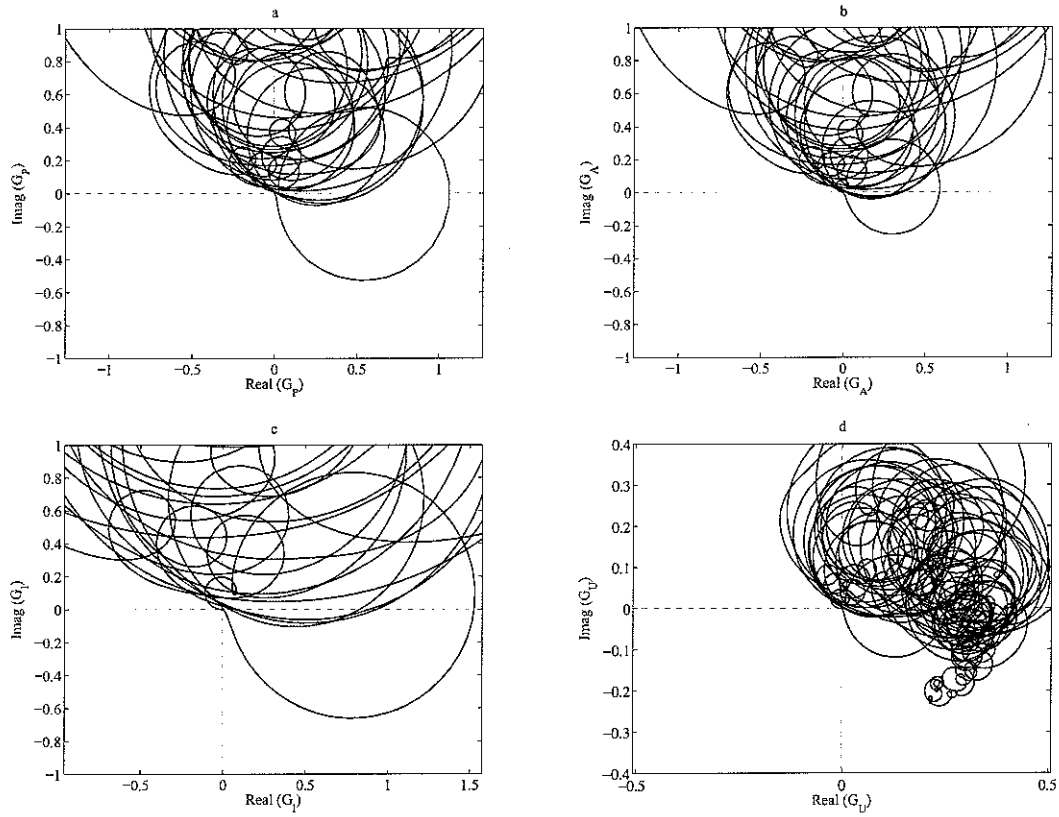

Figure 55: *Nyquist plots of the open loop FRF of the feedback systems using: a) a point force, b) inertial force actuator, inertial electro–dynamic actuator with c) current and d) voltage control in the 1-50 KHz frequency range when a PID control function is used.*

As show in Figure 55 and more in detail in Figure 56, the integral control effect in the PID controller below the first resonance of the plate locates the HY_{cc} locus–circle for the actuator resonance in the top quadrants as seen in Figure 49 and Figure 50 for the purely integral control case. The derivative effect locates the HY_{cc} locus–circle for the first resonance of the plate on the right hand side quadrants as typically happens with proportional control (see Figure 46 and Figure 47). Finally the derivative effect at higher frequency moves the circles to the top quadrants and produces the typical amplification effect proportional to frequency. When the voltage–driven inertial actuator

is used, then, it is found the typical higher frequencies phase lag and amplitude drop which is counterbalanced by the amplification effect of the derivative control.

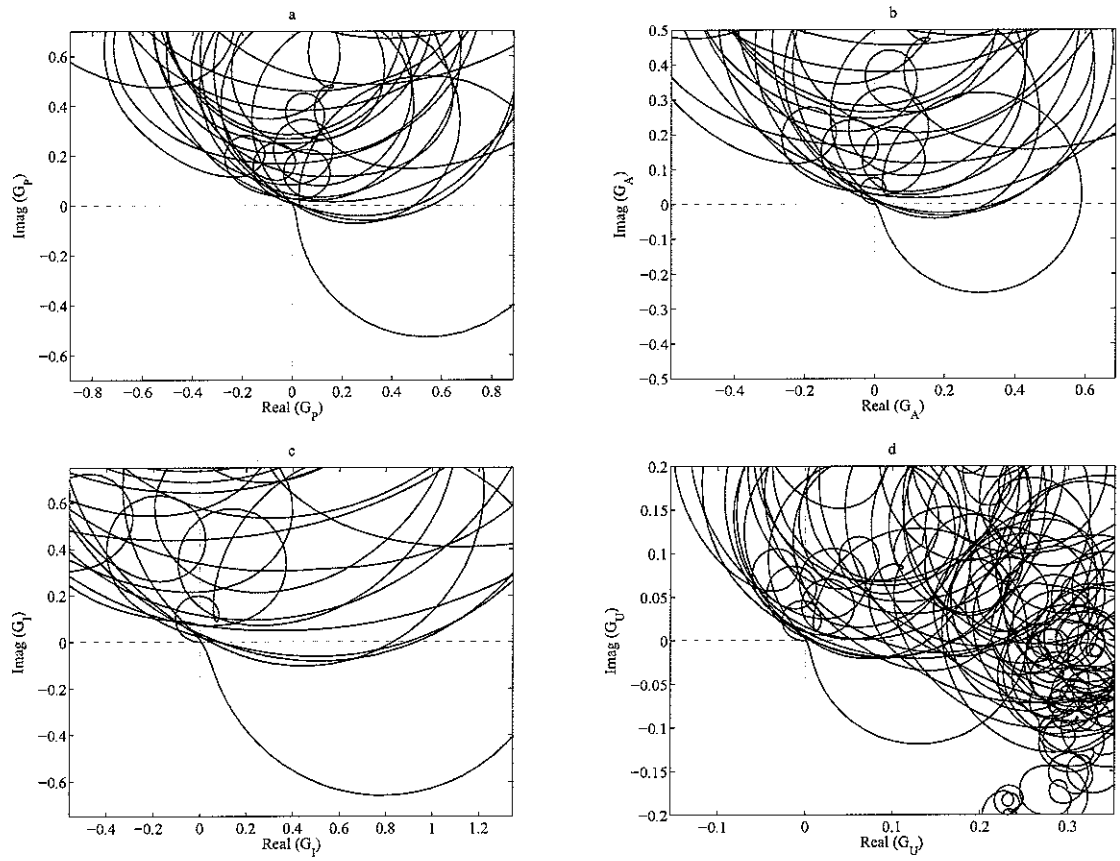

Figure 56: *Zoom of the Nyquist plots show in Figure 55.*

4.6 Control performances.

When distributed flexible systems are considered, such as for example the plate considered in this chapter, then it is convenient to represent the overall vibration of the plate in terms of the total kinetic energy which is given by the following formula:

$$T(\omega)=\frac{1}{2}\int_A \rho h\left|\dot{w}_b(x,y,\omega)\right|^2 dA, \tag{4.81}$$

where ρ is the mass density, h is the thickness of the plate and $\dot{w}_b(x,y,\omega)$ is the transverse velocities on the plate surface. Substituting either Equations (4.77), (4.78), (4.79) and (4.80) into Eq. (4.81), the kinetic energy of the plate is obtained for the four control configurations with either the point force, inertial force actuator or the inertial electro–dynamic actuator; current and voltage driven:

$$T(\omega)=\frac{1}{4}Mf_p^*\left[\mathbf{a}_p+\mathbf{a}_{fc}^{P,A,I,V}\right]^H\left[\mathbf{a}_p+\mathbf{a}_{fc}^{P,A,I,V}\right]f_p, \tag{4.82}$$

where * denotes the complex conjugate, H the hermitian transpose and $\mathbf{a}_{fc}^{P,A,I,V}$ are the column vectors with the modal excitation terms due to the four control loops which are given by:

$$\mathbf{a}_{fc}^{P}=-\mathbf{a}_c\frac{gH(\omega)Y_{cp}}{1+gH(\omega)Y_{cc}}, \tag{4.83}$$

$$\mathbf{a}_{fc}^{A}=-\mathbf{a}_c\left(\mathbf{q}\mathbf{z}_s\frac{gH(\omega)Y_{cp}^{A}}{1+H(\omega)Y_{cc}^{\ A}}+\mathbf{q}\mathbf{Z}\mathbf{y}_p\right), \tag{4.84}$$

$$\mathbf{a}_{fc}^{I}=-\mathbf{a}_c\left(\mathbf{q}\mathbf{z}_s\frac{gH(\omega)Y_{cp}^{I}}{1+H(\omega)Y_{cc}^{\ I}}+\mathbf{q}\mathbf{Z}\mathbf{y}_p\right), \tag{4.85}$$

$$\mathbf{a}_{fc}^{U}=-\mathbf{a}_c\left[\frac{\mathbf{q}\mathbf{z}_s\psi}{Z_e}\left(\left(1-\psi\ \mathbf{h}_t\mathbf{Q}_{cc}\right)\frac{gH(\omega)Y_{cp}^{U}}{1+H(\omega)Y_{cc}^{\ U}}+\psi\ \mathbf{h}_t\mathbf{Q}_{cp}\right)+\mathbf{q}\mathbf{Z}\mathbf{y}_p\right]. \tag{4.86}$$

In the following points the kinetic energy is plotted against frequency for the different control functions.

§ Proportional Control.

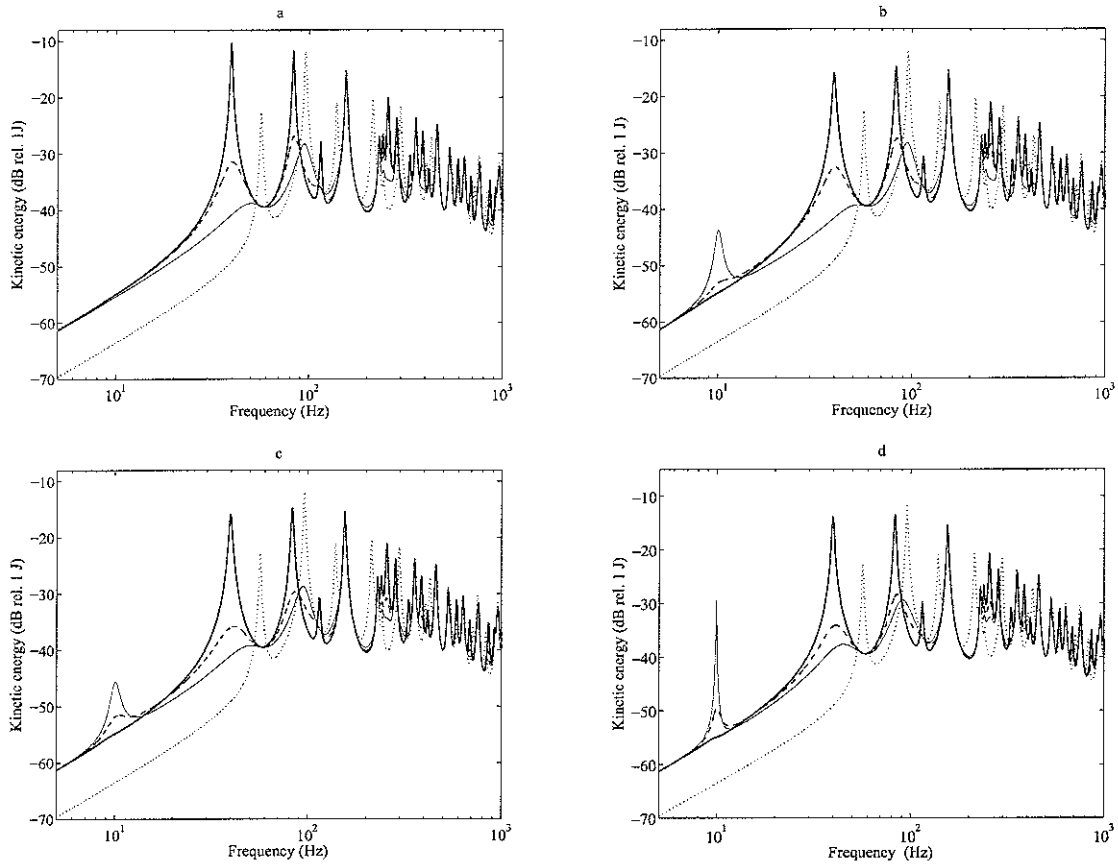

Figure 57: *Total flexural kinetic energy of the plate, when it is excited by an unit primary force using a) a point force, b) inertial force actuator, inertial electro–dynamic actuator with c) current and d) voltage control with no control gain; g_1=0, solid line, having a feedback gain of g_2; dash line, and its optimal g_3 gain; fine line and very high gain; g_4= 10^6; dotted line when a Proportional Control is used.*

Figure 57 shows the active damping effect and the rearrangement of the modal responses of the plate when the gain of the control loop increase. From these plots it is possible to highlight important features of this control system; a) there is an optimal gain that reduces the kinetic energy substantially, b) with relatively larger gains than the optimal value, the system rearranges its modal response so that new resonances come into sight and c) in the case of the system with the inertial actuator mounted on the plate (Figure 57b, c and d) the addition of high gains lead to spillover at the resonance frequency of the actuator. This characteristic behaviour is represented in Figure 58 where the minimum value of the ratio between the 0–1 kHz frequency averaged kinetic energy of the plate with and without feedback control is found for an optimal gain while for bigger gains than this one the ratio of the kinetic energies increases.

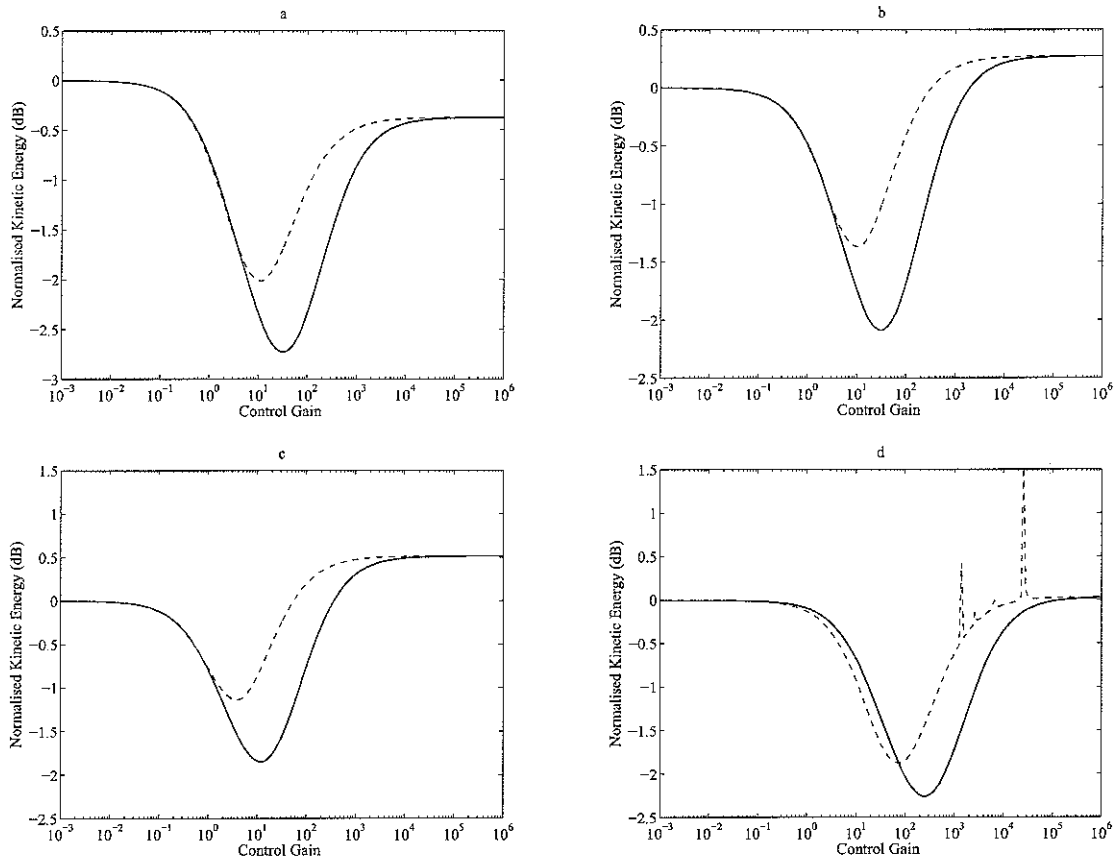

Figure 58: *Ratio of the plate total kinetic energy without and with feedback control integrated from 0 to 1000 Hz, plotted against the gain in the feedback controller, g, for the a) point force, b) inertial force actuator, inertial electro–dynamic actuator with c) current and d) voltage control and for the following feedback control functions; Proportional; fine line, PID; dash line.*

Figure 58 shows that the proportional feedback gives the best 0–1KHz frequency averaged control effect whereas PID is the optimal function 0–100 Hz frequency averaged control effect.

Table 8: *Optimal gains and normalised kinetic energy reduction for the ratio between 0 to 1KHz.*

	Point Force		Actuator		Current Control		Voltage Control	
Proportional	33.31	-2.7dB	33.21	-2.1dB	11.76	-1.8dB	255.29	-2.3dB
PID	11.76	-2.0dB	10.59	-1.8dB	3.74	-1.1dB	76.63	-1.9dB

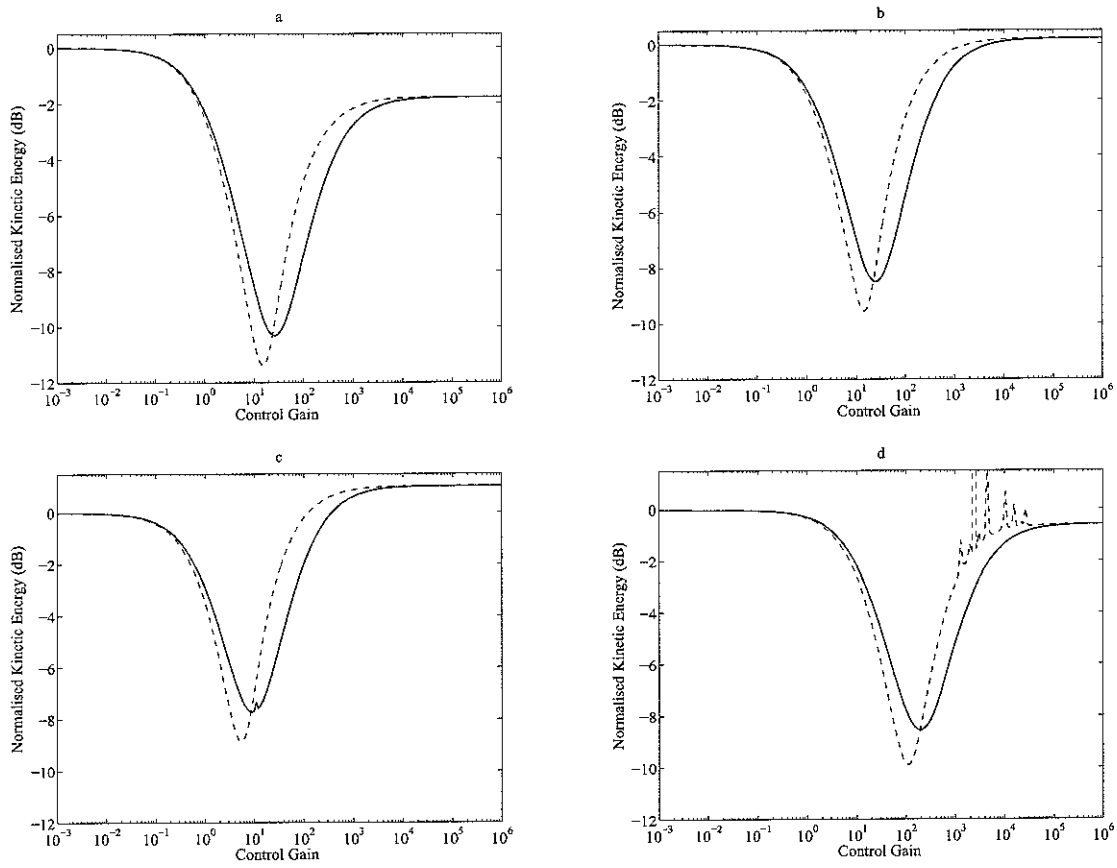

Figure 59: *Ratio of the plate total kinetic energy without and with feedback control integrated from 0 to 100 Hz, plotted against the gain in the feedback controller, g, for the a) point force, b) inertial force actuator, inertial electro–dynamic actuator with c) current and d) voltage control and for the following feedback control functions; Proportional; fine line, PID; dash line, PI; dash-dotted line and PD; dotted line.*

Table 9: *Optimal gains and normalised kinetic energy reduction for the ratio between 0 to 100 Hz.*

	Point Force		Actuator		Current Control		Voltage Control	
Proportional	24.37	-10.3dB	24.37	-8.5dB	8.6	-7.7dB	195.64	-8.5dB
PID	14.48	-11.4dB	14.48	-9.6dB	5.1	-8.7dB	104.73	-9.9dB

§ Integral Control.

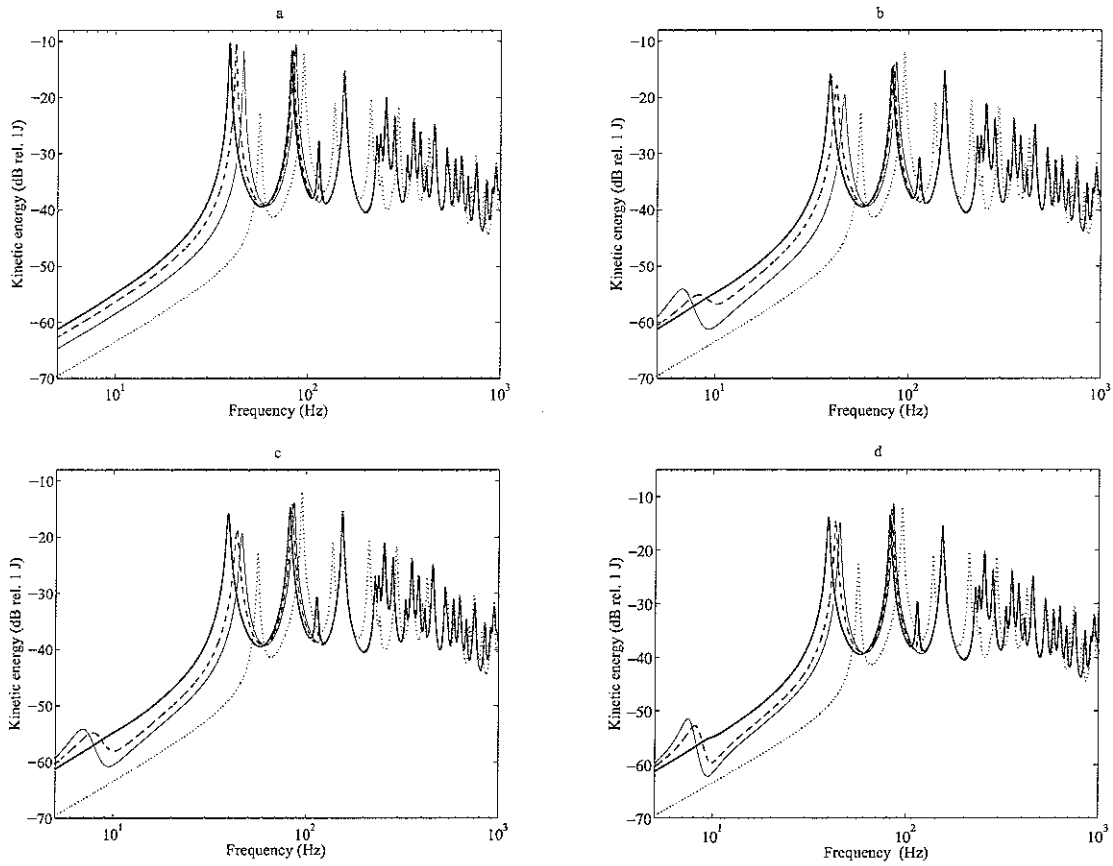

Figure 60: *Total flexural kinetic energy of the plate, when it is excited by an unit primary force using a) a point force, b) inertial force actuator, inertial electro–dynamic actuator with c) current and d) voltage control with no control gain; g_1=0, solid line, having a feedback gain of g_2; dash line, and its optimal g_3 gain; fine line and very high gain; g_4= 10^6; dotted line when a Integral Control is used.*

Figure 60 shows the Active stiffness effects produced by the integral controller and the rearrangement of the modal responses of the plate when the gain of the control loop increases. From this figures it is possible to underline that the addition of even small amounts of control gain moves the resonance frequency of the plate to higher values and the resonance of the actuator to lower values (Figure 60b, c and d). Thus, the system produces vibration reduction at low frequencies below the first resonance of the plate. Also for the case where the inertial actuator is used, spillover is generated on the resonance of the actuator as indicated by the Nyquist plot in Figure 49.

§ Derivative Control.

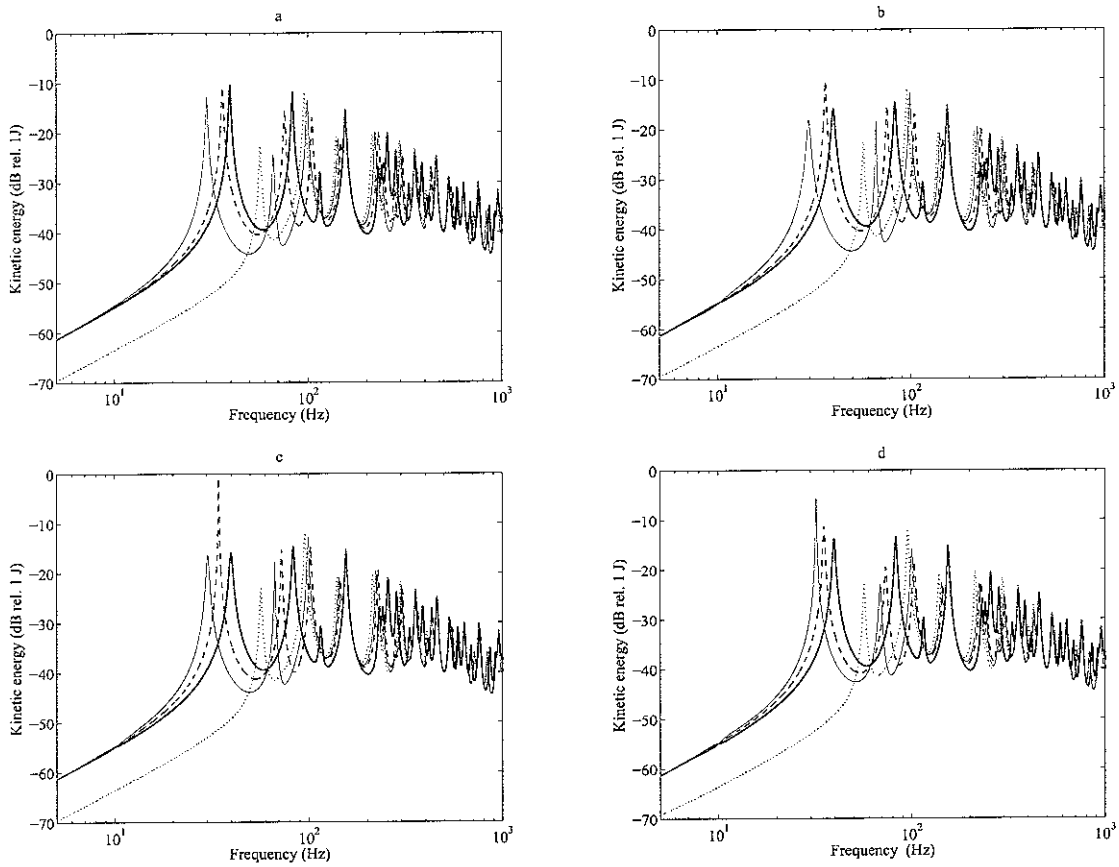

Figure 61: *Total flexural kinetic energy of the plate, when it is excited by an unit primary force using a) a point force, b) inertial force actuator, inertial electro–dynamic actuator with c) current and d) voltage control with no control gain; g_1=0, solid line, having a feedback gain of g_2; dash line, and its optimal g_3 gain; fine line and very high gain; g_4= 10^6; dotted line when a Derivative Control is used.*

In this case, Figure 61 shows that Derivative control adds "Active mass" to the system; moving to lower values the resonances frequencies of the plate. Vibration reduction is produced only between the first and second resonance of the plate.

§ Proportional–Integral–Derivative (PID) Control.

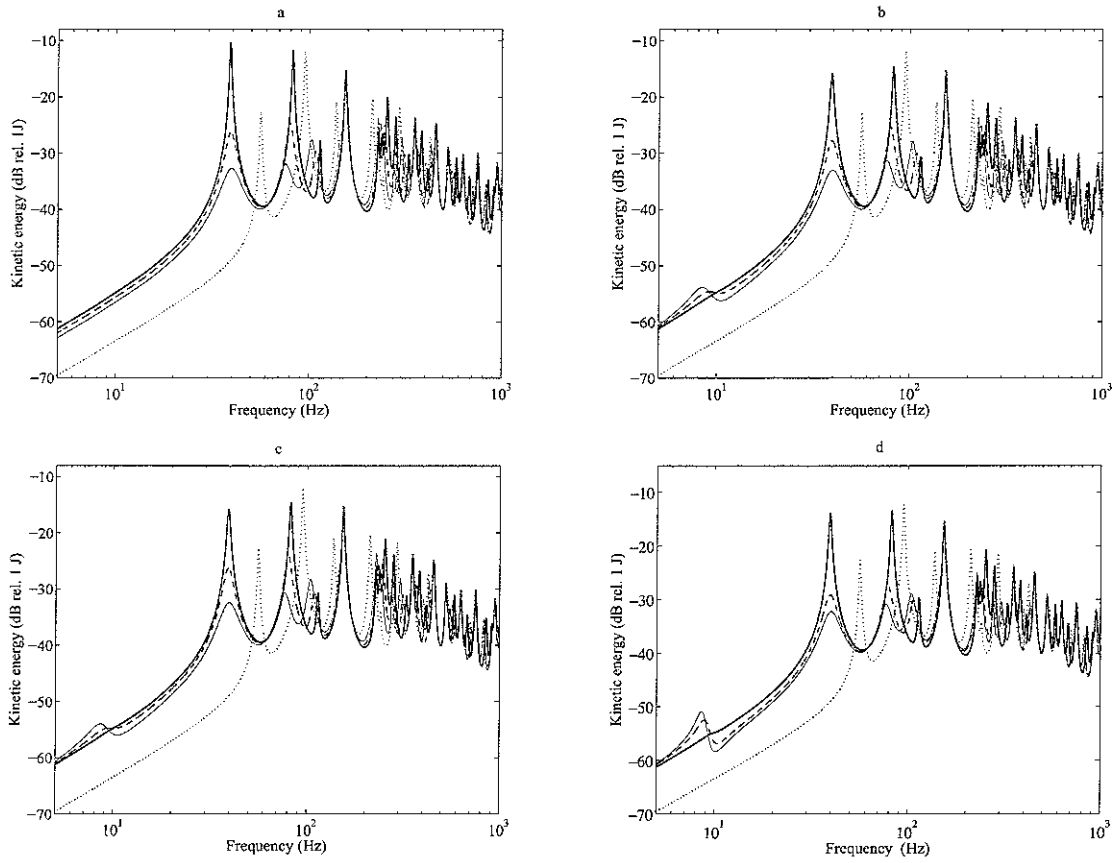

Figure 62: *Total flexural kinetic energy of the plate, when it is excited by an unit primary force using a) a point force, b) inertial force actuator, inertial electro–dynamic actuator with c) current and d) voltage control with no control gain; g_1=0, solid line, having a feedback gain of g_2; dash line, and its optimal g_3 gain; fine line and very high gain; g_4= 10^6; dotted line when a PID Control is used.*

Figure 62 highlights that Proportional–Integral–Derivative control adds; a) Active stiffness at low frequencies below the first resonance frequency of the plate; obtaining vibration reduction in this region, b) Active damping near the first resonance of the plate; controlling the vibration reduction near the first resonance frequency of the plate and c) Active mass at higher frequency, above the first resonance frequency of the plate; achieving vibration reduction at higher frequencies up to the second resonance of the plate. Also it is possible underline that at higher frequencies above the first resonance of the plate, the control system adds "Active mass" moving down the resonances frequencies of the higher order modes. Also for the case where an inertial actuator is mounted on the simple supported plate (Figure 62b, c and d), the actuator resonance is moved down due to the Integral control effect at low frequency As a result much smaller spillover effects are obtained when large control gains are implemented.

4. CONCLUSION.

This report has presented the modelling of different feedback control systems where inertial actuators are used in smart panels for ASAC control. For each system, the effect produced by velocity, displacement, acceleration, a combination among the three or between two of them control loops have been considered in detail. The introductory study on a SDOF system has shown that a) Proportional control implements velocity feedback control; controlling the vibration respond at resonance, b) Integral control implements displacement feedback control; reducing vibration at low frequencies below the resonance, c) Derivative control implements acceleration feedback decreasing the vibration at higher frequencies above resonance, and d) PID Control implements a combination of velocity–displacement–acceleration reducing the vibration below, at and above resonance.

In the chapter 2, the simplest vibration control problem is considered, which consists of a simple degree of freedom (SDOF) system under harmonic motion of the base. In this chapter the inconveniences of using a passive control and the advantages of employing active control are highlighted. Passive control shows that the addition of small amounts of damping leads to important reductions of the response at resonance but also detriment the response at higher frequencies. However, the effects of active control depend on which control function is implemented. For instance the vibration response could be reduced at resonance (Proportional Control, i.e. active damping), below resonance (Integral Control, i.e. active stiffness), above resonance (Derivative Control, i.e. active mass) and below, at and above resonance (PID Control, i.e. active damping–stiffness–mass) without detriment in the others regions. However the control performances of theses loops are limited by stability. Proportional and PID control are unconditionally stable not crossing the real axis while Integral and Derivative Control are also unconditionally stable crossing the real axis and could lead to instabilities and spillover respectively at higher or lower frequencies.

Chapter 3 introduces the control of a SDOF mechanical system with an inertial actuator. As an example, the SDOF system to be controlled could be a simplified model of a simple supported plate taking into account just one mode of vibration. In this case, stability problems due to the actuator dynamics appeared, since the actuator adds a new resonance frequency which produces an extra 180° phase lag in the sensor–actuator frequency response function. In order to reduce this stability problem, this resonance should be much lower than the resonance to the system to be controlled.

Chapter 4 deals with feedback control in a plate. In the first part of this chapter, a simple supported plate with an ideal point force actuator is considered. In this case,

the system is unconditionally stable for all the control systems; however spillover effects are produced for the integral and derivative control systems. In the following parts of this chapter, the point force is substituted by an inertial force actuator or inertial electro–dynamic actuator with either current or voltage control, which adds a new resonance frequency lower than the first mode of the plate. This actuator adds instabilities problems for most of the control schemes. In general, the system will be just conditionally stable for the proportional control system while it will be unconditionally stable for the rest of the control systems. However spillover problems appear for all the control systems.

ACKNOWLEDGEMENTS

This project is supported by the "Early Stage Training site Marie Curie" programme for the "European Doctorate in Sound and Vibration Studies" (EDSVS) which is funded by the European commission.

LIST OF REFERENCES

[1] F.J.Fahy, *Sound and Structural Vibration* London: Academic Press, 1985.

[2] P.A.Nelson and S.J.Elliott, *Active Control of Sound* New York: Academic Press, 1992.

[3] S.J.Elliott, *Signal Processing for Active Control*, 1 ed. London: Academic Press, 2001.

[4] A.Preumont, *Vibration control of active structures*, 2 ed. London: Kluwer Academic, 2002.

[5] Elliott, S. J., Gardonio, P., Sors, T. C., and Brennan, M. J., *"Active vibroacoustic control with multiple local feedback loops,"* The Journal of the Acoustical Society of America, vol. 111, no. 2, pp. 908-915, Feb.2002.

[6] J.Q.Sum, *"Some observations on physical duality and collocation of structural control sensors and actuators,"* Journal of Sound and Vibration, vol. 194 pp. 765-770, 1996.

[7] M.J.Balas, *"Direct velocity control of large space structures,"* Journal of Guidance and Control, vol. 2 pp. 252-253, 1979.

[8] M.E.Johnson and S.J.Elliott, *"Active control of sound radiation using volume velocity cancellation,"* Journal of the Acoustical Society of America, vol. 98 pp. 2174-2186, 1995.

[9] Gardonio, P., Lee, Y. S., Elliott, S. J., and Debost, S., *"Analysis and measurement of a matched volume velocity sensor and uniform force actuator for active structural acoustic control,"* Journal of the Acoustical Society of America, vol. 110, no. 6, pp. 3025-3031, 2001.

[10] Gardonio, P. and Elliott, S. J., *"Modal response of a beam with a sensor-actuator pair for the implementation of velocity feedback control,"* Journal of Sound and Vibration, vol. 284, no. 1-2, pp. 1-22, June2005.

[11] L.Meirovitch, *Dynamics and Control of Structures* New York: John Wiley & Sons, 1990.

[12] C.Paulitsch, *"Vibration Control with electrodynamic actuators."* PhD ISVR, University of Southampton, 2005.

[13] Benassi, L. and Elliott, S. J., *"Active vibration isolation using an inertial actuator with local displacement feedback control,"* Journal of Sound and Vibration, vol. 278, no. 4-5, pp. 705-724, Dec.2004.